DESIGN, MODELING AND SIMULATION OF PLANAR WAVEGUIDE OPTICAL POWER SPLITTER

DESIGN, MODELING AND SIMULATION OF PLANAR WAVEGUIDE OPTICAL POWER SPLITTER

By

Min Huang, B. SC.

A Thesis

Submitted to the School of Graduate Studies

in Partial Fulfillment of the Requirements

for the Degree

Master of Applied Science

McMaster University

© Copyright by Min Huang, July 2008

MASTER OF APPLIED SCIENCE (2008)	McMaster University
Electrical and Computer Engineering	Hamilton, Ontario

TITLE: Design, Modeling and Simulation of Planar Waveguide Optical Splitter

AUTHOR: Min Huang

B. S

(Huazhong University of Sci. & Tech., 2002)

SUPERVISOR: Dr. Xun Li

Professor, Department of Electrical and Computer Engineering

B. Sc. (Shangdong University)

M. Sc. (Wuhan Research Inst. of Posts & Telecom.)

Ph. D. (Northern JiaoTong University)

NUMBER OF PAGES: x, 79

Abstract

1-by-N optical power splitters are primary components in the field of integrated optics and optical transmission systems. Planar waveguide optical power splitters are key devices to realize low-cost optical transmission systems through photonic integration. The goal of this thesis is to design, model and simulate a novel planar waveguide optical power splitter for optical transmission systems and Fiber to the Home (FTTH) networks.

The first chapter is an introduction. This chapter gives the background of power splitter, reviews the existing devices and explains why our novel design is needed.

The idea of this novel power splitter is presented in Chapter 2, including analytical formulations, theoretical calculations and designs. This serves as a theoretical foundation for the development and verification of different parts presented in Chapter 3. The novel power splitter design is composed of a series of waveguide lenses and waveguide phase shifts. The analytical formulations are derived and intensive numerical simulations are performed to verify and investigate this new power splitter. Also the conventional Beam Propagation Method (BPM) is studied in this chapter, which provides a numerical preparation for the device simulation and design in the subsequent chapter.

The design results are shown in Chapter 4. The novel power splitter design predicts good performance with more compact device size, better output

and smaller wavelength dependence. This chapter demonstrated the possibility of new power splitter working as a better approach to the existing MMI or other structures.

Finally, Chapter 5 gives a conclusion to this thesis. The limitations of this work are presented and the future works are proposed.

Acknowledgements

This work would not have been possible without the enormous support and great encouragement from my supervisor, Dr. Xun Li, who has offered me his expert guidance, invaluable advice, numerous help and remarkable patience in various aspects throughout the entire course of my M.A.Sc. program.

I also would like to express my sincere gratitude to Dr. Wei-Ping Huang and Dr. Shiva Kumar for their constant encouraging, enlightening discussions and suggestions and for teaching three important courses on photonic device & system. I am also grateful to the department chair Dr. Kon Max Wong for all his kind help and support and to the graduate assistant Ms. Cheryl Gies for her various help during my two years at McMaster.

I would give special thanks to Dr. Guirong Zhou, the BPM program she wrote before did me a great help. I am also appreciative to my colleagues, Dimitry Labukhin, Ranjbaran Mehdi, etc. for useful discussions. Special thanks to Yi Lan for her kind assistance on preparing the hardcopy of the thesis.

Last but not least, I would like to thank my parents and other family members for their lifelong encouragement and support.

Contents

List of Figures

List of Tables

Chapter 1

Introduction

1.1 Motivation

The ever-increasing bandwidth requirements for Internet services and the promise of broadband links to homes are constantly pushing the telecommunication and data communication systems to higher frequencies and higher bit rates. Fiber optic communication is the key answer to this ever-growing demand for data transmission capacity. The traditional optical communication system employs the “point-to-point” link, which limits the transmission capacity by the speed of the electronic signal processing components, such as electronic router and switching. A passive optical network [1] (PON) is a point-to-multipoint, fiber to the premises network architecture, in which unpowered optical splitters are used to enable a single optical fiber to serve multiple premises, typically 32-128. A PON consists of an Optical Line Termination (OLT) at the service provider's central office and a number of Optical Network Units (ONUs) near end users. A PON configuration reduces the amount of fiber and central office equipments required compared with point to point architectures.

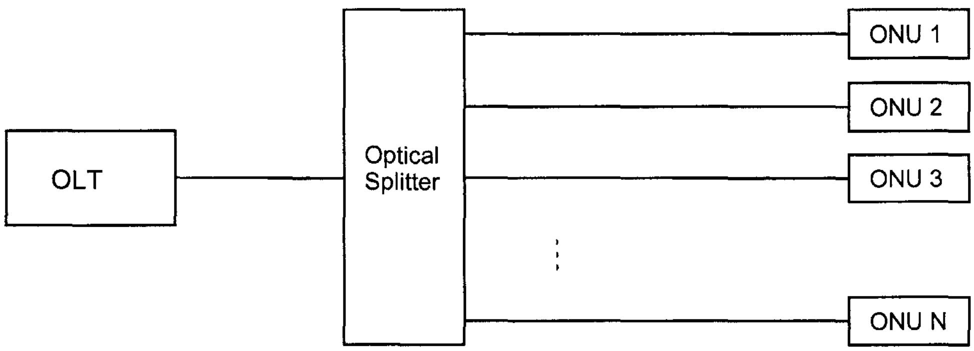

Fig. 1.1 Schematic view of the function of optical splitter for PON and FTTH application

Key optical components in PON systems are optical splitters, which perform the function of splitting optical signals into many channels. As seen in Figure 1.1, an incoming signal passes through an optical splitter. The same signals are then directed to N different spatial channels for further processing. This type of network is good for distribution purposes (for instance Cable-TV) Insertion loss, uniformity, size and cost are important parameters for these splitters.

1.2 Reviews of the Existing Splitter Structures

1.2.1 Waveguide Branches Cascade

Fused bundle of optical fibers [2] can be used when the splitting number is small (N<16). But for large numbers of splitting, integrated optical solutions provide better performance. The simplest way would be making it as a cascade of 1-by-two waveguide branches [3].

Fig. 1.2 shows the schematic view of a silica based splitter [4]. As we can see, the size of the device gets huge as the number of splitting increases. When the number of channels comes to be 32, the length becomes 28mm.

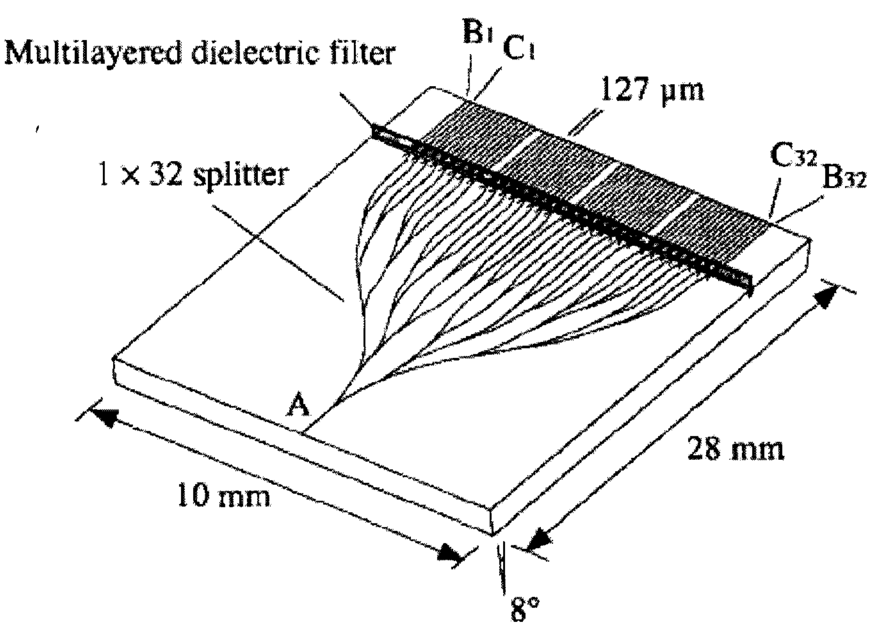

Fig. 1.2 Silica based 1 by 32 splitter

Fig. 1.3 shows a comparison between theoretical and experimental results for a typical 1 by 16 splitter [5]. This 1 x 16 power splitter is 20 mm in length. The theoretical results are shown as a solid curve and the experimental points are shown as two sets of symbols. The two different symbols represent the maximum and minimum insertion loss measured as functions of input polarization state. The theoretical curve includes an assumed propagation loss of 0.3dB/cm and a fiber waveguide modal mismatch loss of 0.5 dB. The device has an insertion loss of 18.9dB, which includes an intrinsic splitting loss of 12 dB.

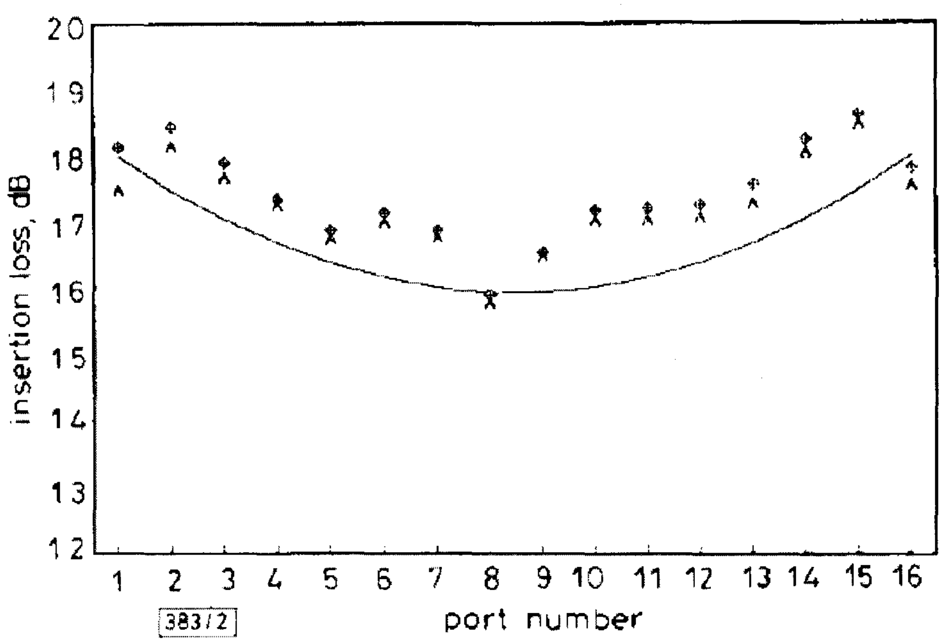

Fig. 1.3 Insertion loss of 1 x 16 power splitter

From the theoretical modeling, optimized 1 x 16 power splitters based on the above approach also have an intrinsic uniformity of 2.1 dB

The processing of the branching point, where the two waveguides start to separate, is technologically very difficult [6]. This generally leads to problems of the uniformity over all the output waveguides and uniformity among different samples.

1.2.2 Multimode Interference Structures

Multimode interference (MMI) power splitters are potentially shorter and better than their branching-type counterparts.

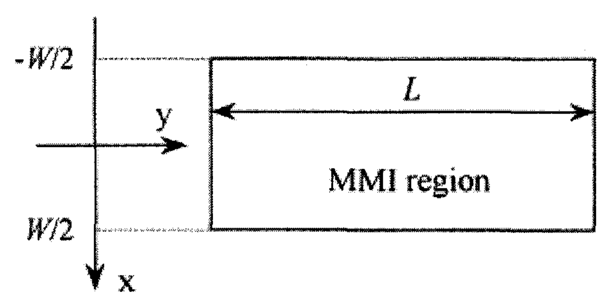

Fig. 1.4 Geometry of an MMI splitter

The common modal of the MMI region is a 3-layer slab waveguide with a core width W and core/cladding refractive index n_c/n_0 [7]. Defining $k=\frac{2\pi}{\lambda_0}$ and using the approximation $k^2n_c^2-\beta_m^2 \ll k^2n_c^2$ [8], the dispersion relationship is given as:

$$\beta_0^a - \beta_m^a = m(m+2)\pi/3L_\pi \tag{1.1}$$

where β_m^a is the propagation constant of mode m. Eq. 1.1 shows the ideal self-imaging effect in slab waveguides. L_π in Eq. 1.1 is the beat length of the two lowest-order modes which can be expressed as:

$$L_\pi \approx \frac{4n_c W_{e0}^2}{3\lambda_0} \tag{1.2}$$

where W_{em} and λ_0 represent the effective mode width of the mth mode and wavelength, respectively.

The MMI length L_{theory} of previous theory can be expressed

$$L_{theory} = \frac{3L_\pi}{4N} \tag{1.3}$$

where N is the number of splitting channels.

In one case [9], $n_c/n_0 = 3.5/3.476$ and $\lambda_0 = 1.55\mu m$, The loss (LS) of 1 by N MMI coupler is:

$$LS = -10\log_{10}(\sum_{n=1}^{N} P_n/P_{in}) \tag{1.4}$$

where P_n and P_{in} represent power of the n_{th} port and input power, respectively. The uniformity (UF) can be given:

$$UF = -10\log_{10}(P_{\min}/P_{\max}) \quad (1.5)$$

with $P_{\min}$ and $P_{\max}$ are the minimum and maximum power of the N ports, respectively. Numerical calculation on loss and uniformity of symmetrical 1 by N MMI power splitter is carried out and the results are listed in table 1.1.

Numerical results of different index contrast with $\lambda_0 = 1.55$ μm, $n_c = 3.5$

W (μm)	n_0	$L = L_{OPT}$ (μm)	LS (dB)	UF (dB)
320(1 × 32)	3.472/3.487	7269/7307	0.0892/0.2422	0.0826/0.2957
160(1 × 16)	3.456/3.480	3647/3677	0.0215/0.1023	0.0063/0.1430
80(1 × 8)	3.430/3.469	1835/1858	0.0206/0.0434	0.0033/0.0408
40(1 × 4)	3.390/3.450	926/941	0.0144/0.0159	0.0033/0.0017
20(1 × 2)	3.327/3.421	471/482	0.0121/0.0157	–

Table 1.1 Simulation results for MMI structure power splitters

Evidently, the length of the multimode section increases linearly with the number of splitting.

1.2.3 Goal of this thesis

The goal of this thesis is to design, model and simulate a planar waveguide optical power splitter for PON communication systems and FTTH networks. Proposing of this novel power splitter is demanded aiming at more compact size, less fabrication cost and higher performance comparing with the conventional MMI.

Challenging tasks of this research topic include:

1. Initial design on device and prove analytical formulism.
2. Employ numerical tools on initial design to prove design concept.
3. Perform efficient optimizations on device design.

1.3 Outline of the Thesis

This thesis contains five chapters together. Fig. 1.5 shows the organization of the five chapters and their relevance to each other. The 1st chapter is an introduction of the research background. Starting from Chapter 2, we begin the main part of the thesis: device design and simulation. Chapter 2 provides the basic idea and theoretical formulation behind the novel power splitter. Then chapter 3 presents the design and optimization of each part of the device. Chapter 4 gives the simulation results of the whole device. Finally, Chapter 5 concludes the whole thesis and puts forward some future research works.

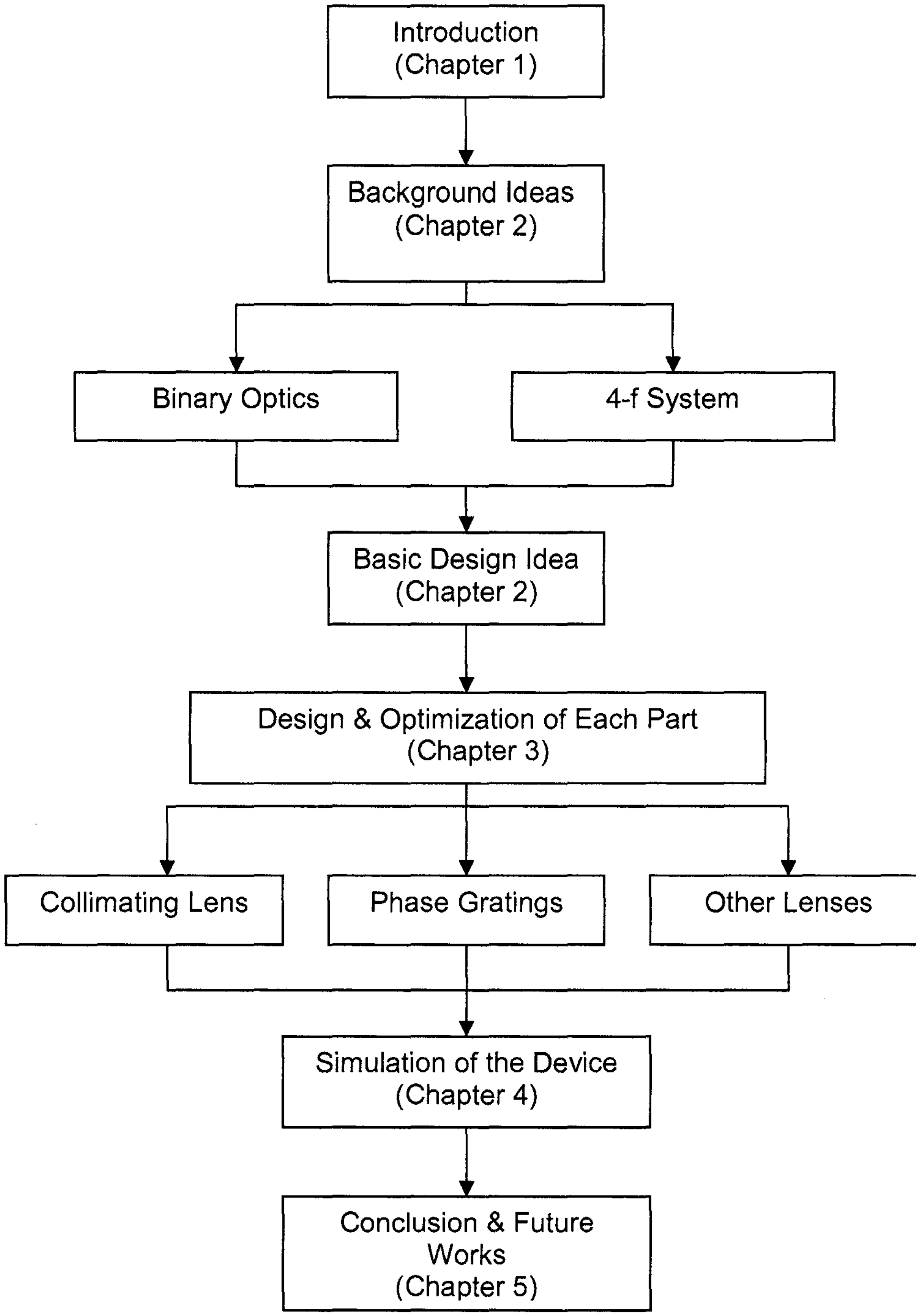

Fig. 1.5 Block diagram of the outline of the thesis

1.4 Contribution of the Thesis

The main contribution of this thesis is the design of a novel planar waveguide power splitter, which composes of carefully designed waveguide lenses and phase gratings. The basic idea comes from phase contrast array illumination [10], and we convert it to planar waveguide platform. The device is proposed and verified by both analytical formulation and numerical simulation.

Chapter 2

Initial Design of the Novel Power Splitter

2.1 Introduction

In this chapter, a novel planar waveguide integrated power splitter is proposed by using a combination of waveguide lenses and waveguide phase gratings. First, the Fourier transforming properties of lenses are reviewed. The 4-f system will be discussed later. Then we introduce the waveguide lenses that are formed by controlling the thickness of the cladding layer which in turn controls the effective index of each area. Finally, the initial design concept of the novel power splitter is explained in section 2.2.3

2.2 Fourier Transforming Properties of Lenses

2.2.1 Fresnel Diffraction

As shown in Fig. 2.1, the diffracting aperture is assumed to lie in the (x,y) plane and is illuminated in the z direction.

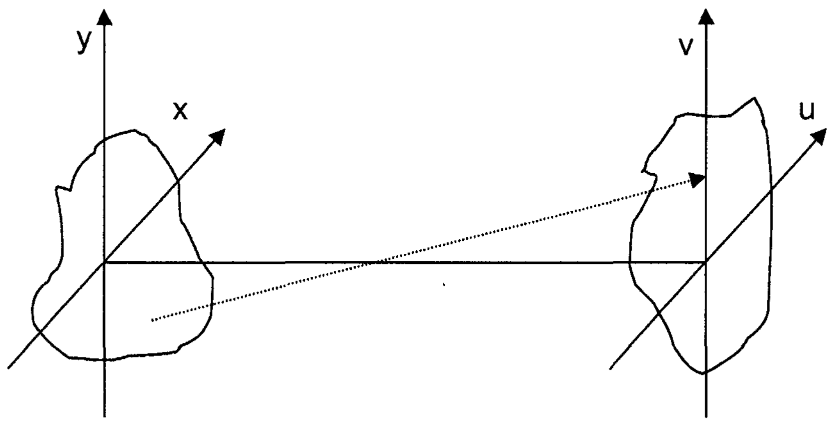

Fig. 2.1 Diffraction geometry

By employing Fresnel diffraction integral [10], we can calculate the wave field across the (u,v) plane, which is parallel to the (x,y) plane and at a distance z to it. The z axis pierces both planes at their origin.

$$U(u,v) = \frac{e^{jkz}}{j\lambda z} e^{j\frac{k}{2z}(u^2+v^2)} \iint \{U(x,y) e^{j\frac{k}{2z}(x^2+y^2)}\} e^{-j\frac{k}{z}(xu+yv)} dxdy \tag{2.1}$$

2.2.2 A Thin Lens as a Phase Transformation

The most important components for optical imaging and data processing systems are lenses. A lens is composed of an optical dense material, in which the propagation velocity is less than the velocity in air. In other words, lens simply delays an incident wavefront by an amount proportional to the thickness of the lens at each point.

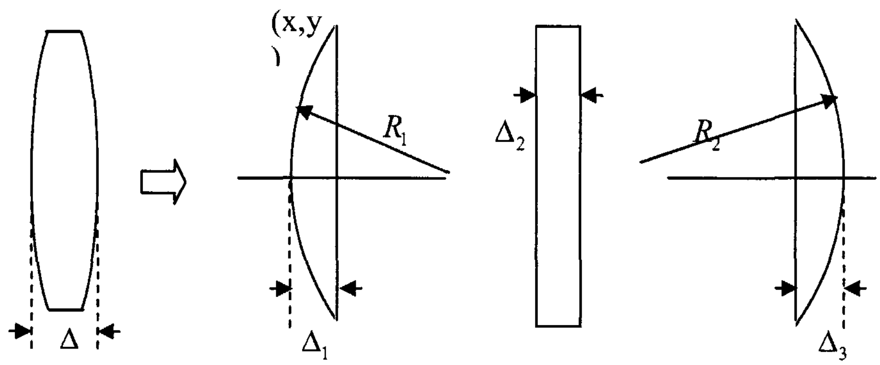

Fig. 2.2 Calculation of the thickness function

In order to calculation the exact phase delay of a lens, we have to get the thickness function. To find the thickness of the lens $\Delta(x, y)$, we split the lens into three parts, as shown in Fig. 2.2.

$$\Delta(x,y) = \Delta_1 + \Delta_2 + \Delta_3 - R_1\left(1 - \sqrt{1 - \frac{x^2 + y^2}{R_1^2}}\right) + R_2\left(1 - \sqrt{1 - \frac{x^2 + y^2}{R_2^2}}\right) \qquad (2.2)$$

Equation 2.2 can be simplified if only the paraxial rays are considered, where we take the approximations of the spherical surfaces of the lens by parabolic surface.

$$\Delta(x,y)=\Delta_1+\Delta_2+\Delta_3-\frac{x^2+y^2}{2}\left(\frac{1}{R_1}-\frac{1}{R_2}\right) \tag{2.3}$$

The phase delay introduced by the lens can be expressed as

$$t(x,y)=e^{jkn(\Delta_1+\Delta_2+\Delta_3)}e^{-jk(n-1)\frac{x^2+y^2}{2}\left(\frac{1}{R_1}-\frac{1}{R_2}\right)} \tag{2.4}$$

Neglecting the constant phase factor, the phase transformation can be rewritten as

$$t(x,y)=e^{-j\frac{k}{2f}\left(x^2+y^2\right)} \tag{2.5}$$

where $\frac{1}{f}=(n-1)\left(\frac{1}{R_1}-\frac{1}{R_2}\right)$

2.2.3 Object in Front of Lens

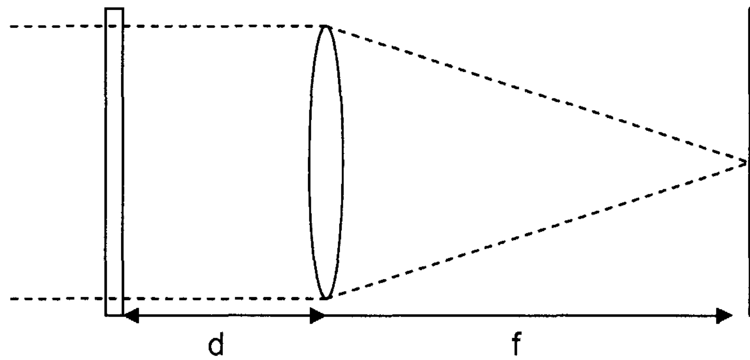

Fig. 2.3 Geometry of the lens system

Consider the optical system of Fig. 2.3. The input, located a distance d in front of the lens, is illuminated by an incident plane wave of amplitude A. We can easily get the amplitude and phase of the light at the back focal plane by using equation (2.1) & (2.5) [10]

$$U(u,v) = \frac{Ae^{j\frac{k}{2f}\left(1-\frac{d}{f}\right)\left(u^2+v^2\right)}}{j\lambda f} \iint t(x,y) e^{-j\frac{2\pi}{\lambda f}(ux+vy)} dxdy \tag{2.6}$$

Evidently when the input is placed in the front focal plane of the lens, where d=f, the phase curvature disappears, leaving an exact Fourier transformation. When the input is placed against the lens, where d=0, the phase curvature introduced can be canceled by a lens of the same shape. Both cases discussed above will be used in the later discuss.

2.3 Spatial Filtering

Spatial filtering is a common method in the process of coherent optics. The idea lies behind it is the Fourier transformation performed by the lens. The final image can be modified by putting a filter properly in the spatial frequency domain, getting rid of some frequency or changing their amplitude or phase.

The Abbe and Porter experiment provides a powerful demonstration of the detailed mechanism by which coherent images are formed, and indeed the most basic principles of Fourier analysis itself [10]. The general nature of these experiments is illustrated in Fig 2.4 (a). An object consisting of a fine wire mesh is illuminated by coherent light. Fourier spectrum of the periodic mesh appears in the back focal plane, and finally in the image plane the various Fourier components passed by the lens are recombined to form a replica of the mesh.

Fig. 2.4 (b) shows the spectrum of the mesh and the full image of the original mesh. The periodic nature of the object generates in the focal plane a series of isolated spectral components. The power of spatial filtering techniques is well illustrated by inserting a narrow slit in the focal plane to pass only a single row of spectral components. Fig. 2.4 (c) shows the transmitted spectrum when a horizontal slit is used. The corresponding image contains only the vertical structure of the mesh; it is precisely the horizontally directed complex-exponential components that contribute to the structure in the image that is uniform vertically.

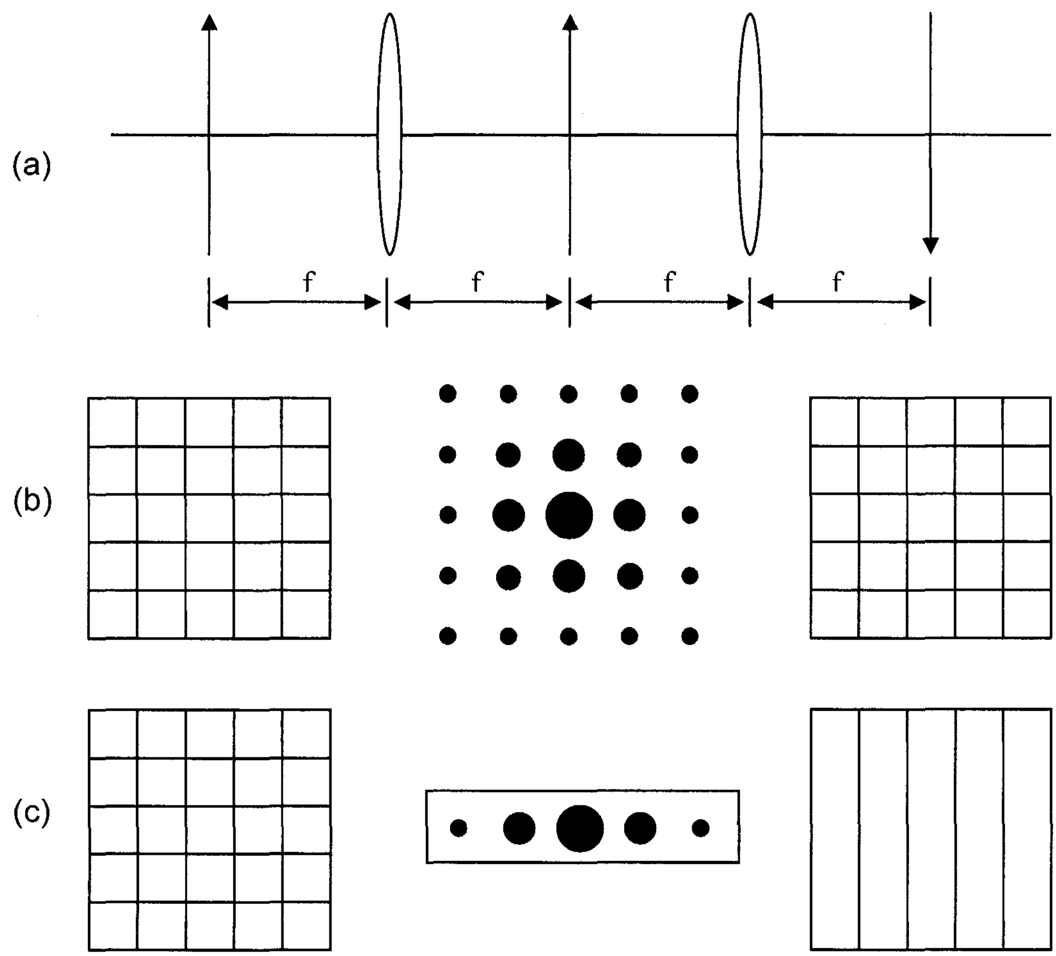

Fig. 2.4 The Abbe-Porter experiment

The spatial filtering system used in this thesis is a 3-f system, as shown in Fig. 2.5, which combines of four lenses: L0 is for collimating light. L1 & L3 are for Fourier transformation. L2 is for phase compensation.

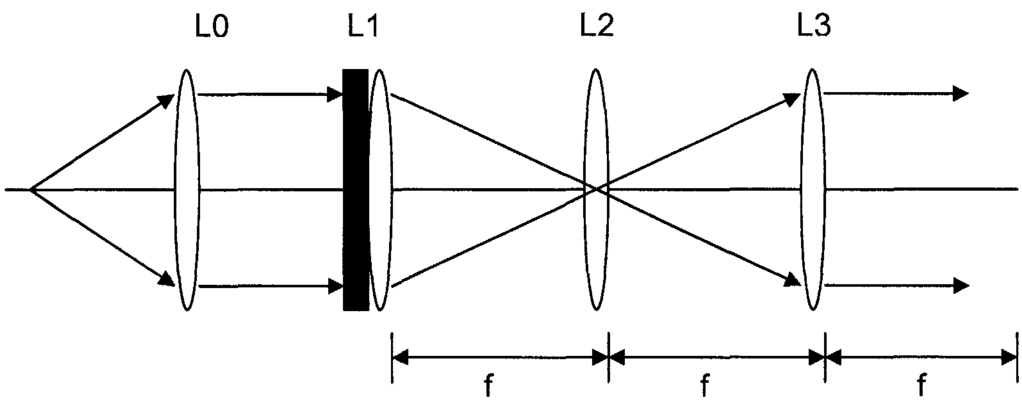

Fig. 2.5 3-f system

2.4 Planar Waveguide Structure

2.4.1 Micro Optics

The terms micro- and nanooptics refer to the typical lateral feature size in an optical element [11]. In the 1960s, the minimum feature size of lithographic fabrication was of the order of tens of micrometers. Fabrication of optical elements was often achieved by using plotters, generating huge patterns on paper or on film that were photo reduced in a subsequent step. The optical elements were called “computer-generated holograms” and used, e.g., for analog optical signal processing [12].

An enormous push towards micro optics came in the 1980s (although the forerunners were from the 1960s and 1970s). At that time, standard lithography offered a feature size of about 1 micrometer. But, importantly, dry etching techniques were adopted to make micro optical devices like, in particular, diffractive optical elements in glass or silicon. Newly developed iterative design techniques allowed one to generate novel types of optical elements such as 1xN beam splitters and lens let arrays [13]. Meanwhile, micro optics is a well-established and mature technology. Micro optical components can be found in various applications, for example, as lens arrays in cameras and displays, as beam splitters and homogenizers in laser systems, as micro-spectrometers in analytics, etc.

Actually the basic idea of the power splitter is common in 3D optics [13]. However, we convert it to our planar waveguide structure which will be discussed latter.

2.4.2 Waveguide-based Integrated Structure

Our novel power splitter is based on planar waveguide structure. The idea here is using the slab waveguide as the 2D version of the classical 3D diffraction optics [25]. The geometry of the structure is shown in Fig. 2.6. The light is confined by the slab waveguide in the x-y plane (the cross-section), and travels along z direction in x-z plane.

There are two different areas in x-z plane: the dark areas are with thicker claddings while the rest is normal slab waveguide, i.e. we create mesa of different shapes on top of the slab waveguide platform. Obviously, the dark areas have higher effective refractive index (n_2) compared with the rest slab waveguide platform (n_1), and the effective refractive index difference can be controlled by changing the height of the mesa. The shape of the mesa determines its function. Here we use InGaAsP/InP systems with 0.4 index difference. The dependence of the refractive index on material composition has been well investigated [14]. Here we make n_1 equal to 3.2, while n_2 equal to 3.6, and the operating wavelength is 1.55 μm.

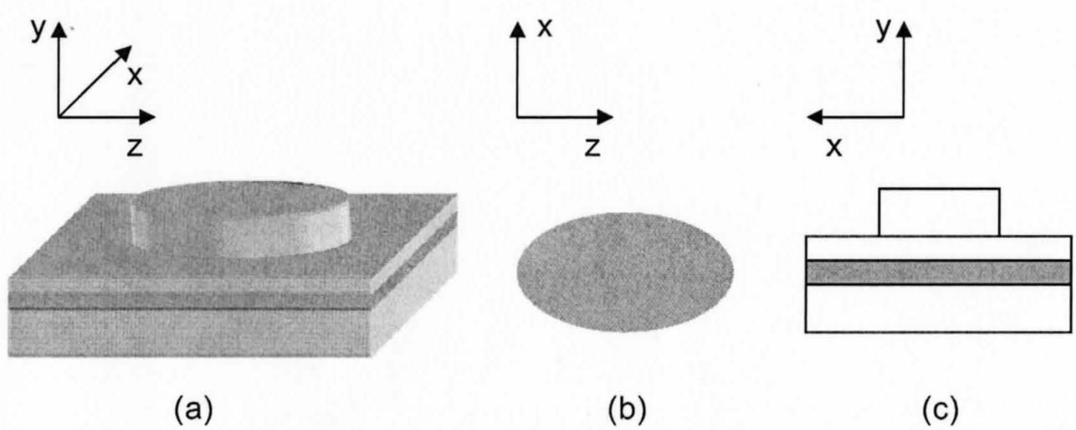

Fig. 2.6 The geometry of waveguide-based integrated structure. (a) is the 3D view, (b) is the top view, and (c) is the side view

Actually the design concept is based on the layout design on 2D (x,z) plane. We can use concepts in 3D optical system in our case. The only difference is that we convert it into x-z plane by making different kinds of mesas.

2.5 Initial Design by Analytical Formulations

The layout design in x-z plane is made on simple Fourier transform (FT) based analysis. As shown in Fig.2.7, Area 1 is an input waveguide, Area 2 is a lens for light beam collimating, Area 3 is a diffraction grating through which light beam will be redirected into different orders, Area 4&7are lenses for FT and inverse FT, Area 5 is for phase compensation, Area 6 is a phase shift part which will introduce a phase delay to the 0^{th} order light beam, and Area 8 is the output waveguides.

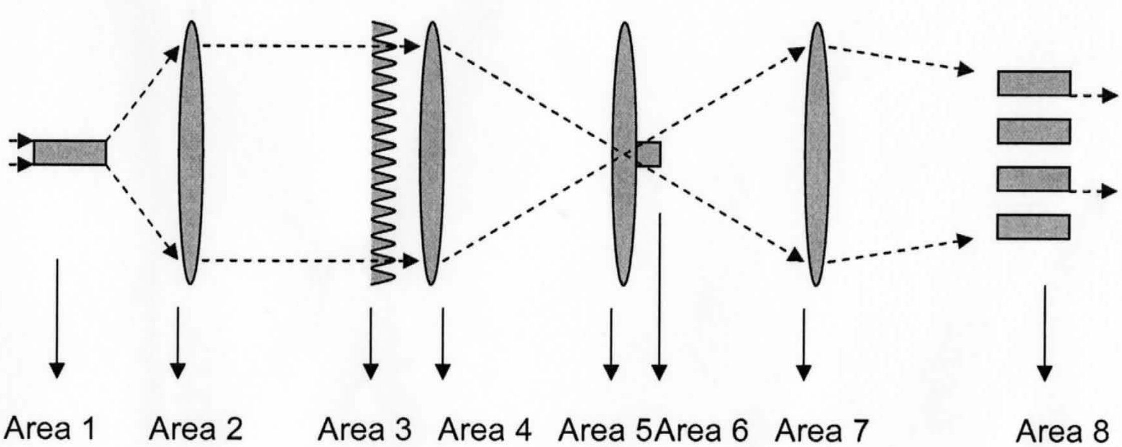

Fig. 2.7 Schematic view of the power splitter

Here we present a simple case to illustrate how the power splitter works. Although some changes have been brought in to optimize the performance in the final design, the basic principle remains the same. Actually, if the whole system is ideal, the field distribution of the light beam $u_1(x)$ after the first lens is simply the FT of the pupil function [10], i.e., the guided mode profile $u_0(x)$ in input waveguide. Since the mode in a single mode ridge waveguide is similar to a pulse function, we can assume $u_1(x)$ to be a plane wave.

delta

$$u_1(x) = F[u_0(x)] \approx Ga(x/D) \tag{2.7}$$

where $F[...]$ indicates FT and $F^{-1}[...]$ indicates inverse FT. And the gate function is defined as

$$Ga(x/D) = \begin{cases} 1, |x| \le \dfrac{D}{2} \\ 0, |x| > \dfrac{D}{2} \end{cases} \tag{2.8}$$

The diffraction grating is designed to be a periodical structure with N periods (N refers to the splitting number). The phase shift φ in a single period T is

$$\varphi(x) = \begin{cases} 0, 0 < x < T/4 \\ \pi, T/4 < x < T \end{cases} \tag{2.9}$$

After the diffraction grating, the field distribution $u_2(x)$ is multiplied by a factor with unit amplitude and a phase shift $\varphi(x)$ along x. Therefore, in one period we have

$$u_2(x) = u_1(x)\exp[j\varphi(x)] = \begin{cases} 1, 0 < x < T/4 \\ -1, T/4 < x < T \end{cases} \tag{2.10}$$

The field distribution is shown in Fig. 2.8.

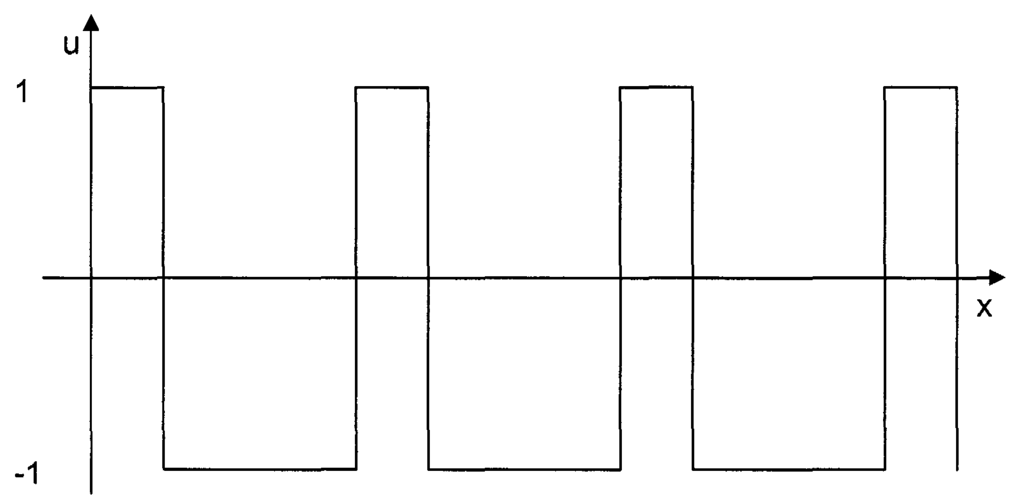

Fig. 2.8 Optical field after phase gratings

Along the focal line of the second lens, the field distribution $u_3(x)$ is obviously the FT of $u_2(x)$:

$$u_3(x) = F[u_2(x)] \tag{2.11}$$

The light beam has been redirected to different orders. The 0^{th} order (DC part), which lies in the center part, can be expressed as

$$u_{0^{th}} = \frac{1}{T}\int_0^T E dx = \frac{1}{T}\left(\int_0^{T/4} 1 dx + \int_{T/4}^{T} (-1) dx\right) = -1/2 \tag{2.12}$$

Then $u_2(x)$ can be expressed as the summation of the DC and AC parts, which is shown in Fig. 2.9.

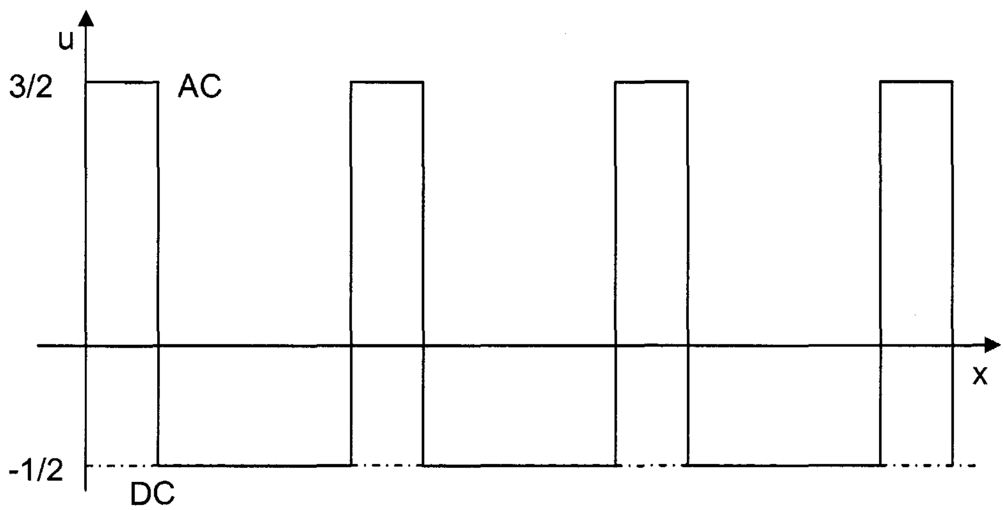

Fig. 2.9 AC and DC part

Then we introduce a π phase delay to the 0^{th} order light beam

$$u_{0^{th}}'(x) = u_{0^{th}}(x)\exp[j\pi] = \frac{1}{2} \tag{2.13}$$

The optical field is shown in fig. 2.10

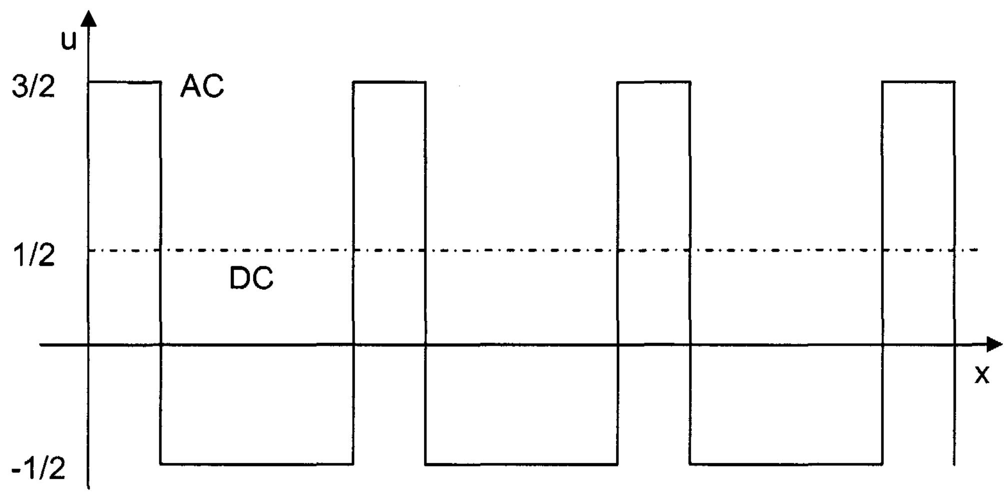

Fig. 2.10 Optical field on the focal plane of the last lens

Like 4-f system in Fourier optics, the last lens is the inverse FT of $u_3(x)$, which refocus the light beam. The field distribution $u_4(x)$ in the focal line will be

$$u_2(x) = \begin{cases} -\frac{1}{2}+\frac{3}{2}, 0<x<T/4 \\ -\frac{1}{2}-\frac{1}{2}, T/4<x<T \end{cases} \Rightarrow u_4(x) = \begin{cases} +\frac{1}{2}+\frac{3}{2}=2, 0<x<T/4 \\ +\frac{1}{2}-\frac{1}{2}=0, T/4<x<T \end{cases} \tag{2.14}$$

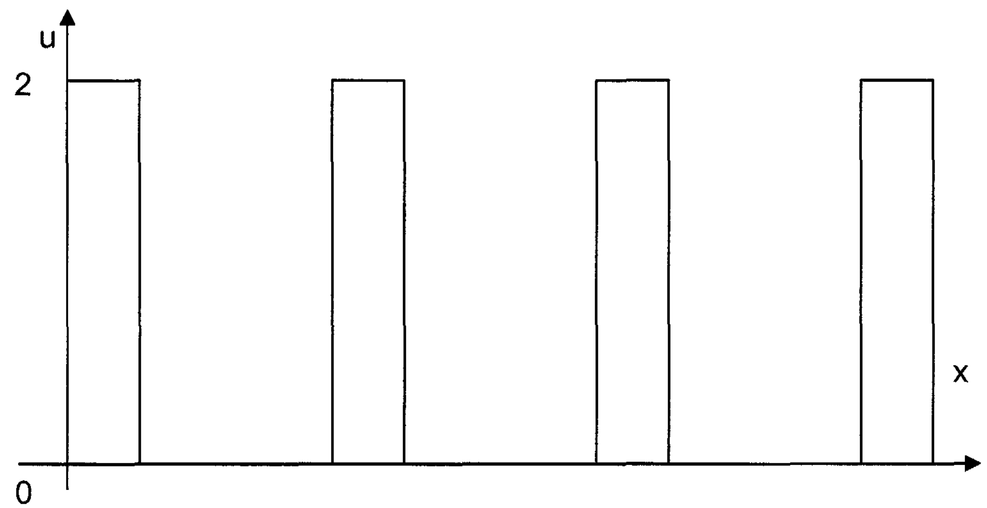

Fig. 2.11 Final output field

The output is shown in Fig. 2.11. This means in ideal case we can only obtain light in ¼ of the period. Along the focal line of the last lens we obtain an ideal power splitter.

2.6 Summary

In this chapter, we reviewed the Fourier transforming properties of lenses, which are the basic ideas behind our design. Then the planar waveguide structure is introduced. By employing different mesa shapes on the structure we can realize the geometry optical propagation in 2D plane. The analytical formulation and design concept are proposed at the end of this chapter. The following chapter (chapter 3) will be the verification and optimization of this concept.

Chapter 3

Numerical Verification and Improved Design by BPM

3.1 Introduction

The basic design concept was proposed in the previous chapter (chapter 2). But there still exists many problems when we put it into practice. For example, the coherent light we considered was a gate function, but it is difficult to design the 1^{st} lens in reality which can collimate the incoming light. Another issue is that the phase grating we proposed was a rectangular period shape, the discontinuity of the corners may cause unwanted diffraction orders on the back focal plane of the 2^{nd} lens.

In this chapter, we design and verify those parts discussed in chapter 2 one by one. First, the concept of beam propagation method (BPM) is presented. Then the mathematical derivations on the major components are provided based on scalar wave propagation and paraxial approximation. After that, the initial design based on this analytical derivation is drawn. Finally, the numerical tool, which is discussed above, is employed to verify and optimize the design. It is found that careful design of both waveguide lenses and phase gratings are crucial to the function of the entire power splitter. We will mainly talk about these two parts.

3.2 Beam Propagation Method

3.2.1 Numerical Methods

Optical waveguides are the simplest but the most important element of photonic integrated devices [15]. Not only are they used for interconnection between the devices but also are building blocks to form various photonic devices. In order to perform design and simulation of planar optical waveguide-based optical splitter, efficient and accurate numerical simulation tools are indispensable. There exist two main categories of problems in simulating optical devices and circuits: optical wave propagation and optical modal analysis.

One of the most commonly used numerical methods for modeling wave propagation is the beam propagation method (BPM). BPM is an approximation technique for simulating the propagation of light in slowly varying optical waveguides. BPM was first introduced in 1970's by Feit and Fleck [16]. When a wave propagates along a waveguide for a large distance (larger compared with the wavelength), rigorous numerical simulation is difficult. The BPM relies on approximate differential equations which are also called the one-way models. These one-way models involve only a first order derivative in the variable z (for the waveguide axis) and they can be solved as "initial" value problem. The "initial" value problem does not involve time, rather it is for the spatial variable z.

The beam propagation method is widely used for modeling and analysis of guided-wave optical devices and circuits. BPM enables us to calculate field amplitude distributions of the light wave that travels through a waveguide in the presence of small refractive index variations. It consists basically of propagating the input beam over a small distance through homogeneous space and then correcting for the refractive-index variations seen by this beam during the propagation step [19]. The calculated result can be visualized in a 3D drawing to show the behavior of the propagating light.

How to get accurate and efficient calculation of optical waveguide modes has always been a popular research topic due to its fundamental importance in design of guided-wave optical devices and circuits. Numerical mode calculation methods include Finite Difference (FD) [17] and Finite Element Method (FEM) [18]. Both of them are based on solving eigen value and eigen equations.

3.2.2 Beam Propagation Method

Starting from the Maxwell equations:

$$\nabla \times \hat{E} = -j\omega\hat{B} = -j\omega\mu\hat{H} \tag{3.1}$$

$$\nabla \times \hat{H} = j\omega\hat{D} = j\omega\varepsilon\hat{E} \tag{3.2}$$

$$\nabla \cdot \hat{H} = 0 \tag{3.3}$$

$$\nabla \cdot \varepsilon\hat{E} = 0 \tag{3.4}$$

Applying a vector rotation operator to (3.1), we get the governing equation for the propagation of the electromagnetic waves in homogeneous medium

$$\nabla \times \nabla \times \hat{E} = -j\omega\mu\nabla \times \hat{H} = k_0^{\ 2} n^2 \hat{E} \tag{3.5}$$

where $k_0 = \omega\sqrt{\varepsilon_0 \mu_0}$, and n is the effective index.

From (3.4) we have

$$\nabla \times \nabla \times \hat{E} = \nabla\left(\nabla \cdot \hat{E}\right) - \nabla^2 \hat{E} = -\nabla\left(\frac{\nabla\varepsilon}{\varepsilon} \cdot \hat{E}\right) - \nabla^2 \hat{E} \tag{3.6}$$

By putting (3.5) & (3.6) together we have

$$k_0^{\ 2} n^2 \hat{E} + \nabla^2 \hat{E} = -\nabla\left(\frac{\nabla\varepsilon}{\varepsilon} \cdot \hat{E}\right) \tag{3.7}$$

Equation (3.7) is valid for most photonic guided-wave devices

Here, the slowly varying envelope approximation is used to approximate the wave function $\hat{E}$ of the light propagation in the +z direction. In this approximation, $\hat{E}$ is separated into the slowly varying envelope function E and the very fast oscillatory phase term $e^{-j\beta z}$ as follows [20]

$$\hat{E}(x,y,z) = E(x,y,z)e^{-j\beta z} \tag{3.8}$$

where $\beta = n_{eff}k_0$, n_{eff} is the reference index, for which the refractive index of the substrate or cladding is usually used

Substitute (3.8) to (3.7), one is able to derive the one-way wave equation

$$\frac{\partial^2 E}{\partial z^2} - 2j\beta\frac{\partial E}{\partial z} + \nabla_\perp^2 E + \left(k_0^2 n^2 - \beta^2\right)E = -\nabla_\perp\left(\frac{\nabla_\perp \varepsilon}{\varepsilon}\cdot E\right) \tag{3.9}$$

where $\nabla_\perp^2$ is a Laplacian in the lateral directions.

The solution to (3.9) is given by

$$\frac{\partial E}{\partial z} = -j\beta(\sqrt{1+P} - 1)E \tag{3.10}$$

where the operator P is defined by

$$PE = \frac{1}{\beta^2}\left(\nabla_\perp^2 E + \left(k_0^2 n^2 - \beta^2\right)E + \nabla_\perp\left(\frac{\nabla_\perp \varepsilon}{\varepsilon}\cdot E\right)\right) \tag{3.11}$$

The BPM program used in this work is a split-step time domain propagation method (SSTD-BPM) [21], which can extend conventional BPM to enable simulating time domain pulse.

The time domain traveling wave equation can be derived from time domain vectorial wave equation [22].

$$\nabla \times \nabla \times \hat{E} - k_0^2 n^2 \hat{E} + 2jnk_0\beta_1 \frac{\partial \hat{E}}{\partial t} = 0 \qquad (3.12)$$

where $\beta_1 = \frac{1}{v_g} = \frac{n_g}{c}$, n_g is group index and v_g is group velocity. Following the similar procedure as described above, it is easy to get:

$$\frac{\partial E}{\partial z} = -j\beta(\sqrt{1+P}-1)E - \frac{n\beta_1}{n_0}\frac{\partial E}{\partial t} \qquad (3.13)$$

The solution to equation (3.13) is

$$E(z+\Delta z, t) = e^{-j\beta(\sqrt{1+P}-1)\Delta z} e^{-\frac{nn_g}{n_0 c}\Delta z \frac{\partial}{\partial t}} E(z,t) \qquad (3.14)$$

To solve equation (3.14) we can introduce an auxiliary variable ψ

$$\psi = e^{-\frac{nn_g}{n_0 c}\Delta z \frac{\partial}{\partial t}} E(z,t) \tag{3.15}$$

Then the solution for equation (3.14) can be handled by the traditional BPM algorithm. We use the higher order Taylor expansion on equation (3.15).

$$\psi = e^{-\frac{nn_g}{n_0 c}\Delta z \frac{\partial}{\partial t}} E(z,t) \approx \frac{1 - \dfrac{nn_g}{n_0 c}\Delta z \dfrac{\partial}{\partial t}}{1 + \dfrac{nn_g}{n_0 c}\Delta z \dfrac{\partial}{\partial t}} E(z,t) \tag{3.16}$$

Apply Crank-Nicolson formula to equation (3.16), we get

$$\begin{aligned} &\frac{\psi(z,t)+\psi(z,t-\Delta t)}{2} + \frac{nn_g \Delta z}{2n_0 c}\frac{\psi(z,t)-\psi(z,t-\Delta t)}{\Delta t} \\ &= \frac{E(z,t)+E(z,t-\Delta t)}{2} - \frac{nn_g \Delta z}{2n_0 c}\frac{E(z,t)-E(z,t-\Delta t)}{\Delta t} \end{aligned} \tag{3.17}$$

Here comes the scheme for temporal solution equation (3.15)

$$\psi(z,t) = -C\psi(z,t-\Delta t) + CE(z,t) + E(z,t-\Delta t) \tag{3.18}$$

where

$$C = \frac{1 - \frac{nn_g}{n_0 c}\frac{\Delta z}{\Delta t}}{1 + \frac{nn_g}{n_0 c}\frac{\Delta z}{\Delta t}} \tag{3.19}$$

3.3 Lens Design

3.3.1 Lens Design Concept

A schematic diagram of a lens structure with an aperture D is shown in Fig. 3.1.

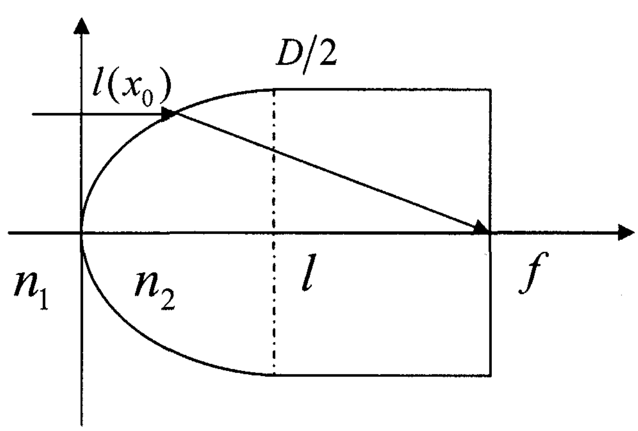

Fig. 3.1 Schematic diagram of a lens structure

The refractive indices inside and outside the lens structure are denoted by n_2 and n_1, respectively. According to the ray optics theory [23], the lens should be shaped in such a way that makes the collimated light coming from left to right focused at point f or vice versa, i.e. optical paths of the rays in the collimated beam should be all equal

$$n_2 f = n_1 l(x_0) + n_2 \sqrt{[f - l(x_0)]^2 + x_0^2} \tag{3.20}$$

The equation above can be rewritten in the following form

$$\frac{[l(x_0) - a]^2}{a^2} + \frac{x_0^2}{b^2} = 1 \tag{3.21}$$

where

$$a = \frac{n_2 f}{n_1 + n_2}$$
$$b = f\sqrt{\frac{n_2 - n_1}{n_1 + n_2}}$$

Obviously the lens takes an elliptical shape with a as the long axis while b as the short one. From (3.20) we can also have

$$l(x_0) = a - a\sqrt{1 - \frac{x_0^2}{b^2}} \approx a - a(1 - \frac{x_0^2}{b^2}) = \frac{a x_0^2}{2b^2} \tag{3.22}$$

where the first order Taylor expansion of the square root is applied under the condition that $\frac{x_0}{b}$ is much smaller than 1. With the inserted lens as a phase shift, the pupil function becomes

$$u(x_0,0)Ga(x/D)e^{j\frac{2\pi}{\lambda}\{n_1 l(x_0)+n_2[l(D/2)-l(x_0)]\}} \tag{3.23}$$

Therefore, the field distribution at the focal line of the lens (z = f) for a given field at the origin (z = 0) is obtained by using (3.23) as the pupil function in Fresnel (near-field) diffraction formula

$$\begin{aligned} u(x,f) &= \sqrt{\frac{n}{j\lambda f}}e^{jkn_2[f+\frac{x^2}{2f}]}\int_{-\infty}^{\infty} e^{jkn_2\frac{x_0^2}{2f}}u(x_0,0)Ga(x/D)e^{jkn_2[l(D/2)-\frac{x_0^2}{2f}]}e^{-jkn_2\frac{xx_0}{f}}dx_0 \\ &= \sqrt{\frac{n}{j\lambda f}}e^{jkn_2[f+\frac{x^2}{2f}+l(D/2)]}\int_{-D/2}^{D/2} u(x_0,0)e^{-jkn_2\frac{xx_0}{f}}dx_0 \end{aligned} \tag{3.24}$$

From equation (3.24), it can be found that the lens plays a role as a spatial Fourier transformer. Through the help of the suitable lens, we can make spatial Fourier transform rule applicable in the near field region. Physically, the lens corrects spherical wave front to plane wave front by forcing the rays with smaller angle (to the propagation axis) to experience more delays. This correction is only valid with the paraxial assumption under which the spherical wave is firstly approximated by a parabolic wave. After such correction, the Fresnel transformation becomes the spatial Fourier transformation without the far-field assumption. Also because of such spherical wave to plane wave correction, a point source at the focal line will be collimated by the lens at its aperture.

Parameters	Value (μm)
n_2	3.6
n_1	3.2
l	213λ
D	194λ
f	415λ

Table 3.1 Parameters for the lens

3.3.2 1st Lens Design

Some certain approximations have been made in the original derivation in order to simply the process. In real design, the waveguide mode is treated instead of the point source. Also, the lens aperture makes the spatial Fourier transform non-ideal. Most importantly, the paraxial approximation is introduced to simplify the derivation. Due to all these approximations, the design obtained previously can not provide accurate enough results for practical application. More precise numerical simulation tools such as wide-angle beam propagation method (BPM) are used to verify and further improve the design.

Firstly, we investigate the function of the waveguide lens numerically. The low and high indices are chosen as $n_1 = 3.2$, $n_2 = 3.6$. Wavelength is chosen as 1.55μm, and the focal length is chosen as f = 415λ = 643μm. The lens shape is designed exactly from the equations above: a = 213λ = 330μm, b = 97λ = 150μm. The input and output waveguides are chosen as width as 2.0μm with a 0.2 index difference between the core and cladding.

In order to show the collimation function of the lens in a clearer way, we record both the amplitude and effective along z-direction and plot them in Fig. 3.2 & Fig. 3.3. The effective phase constant is defined as

$$\varphi_{eff} = -j\left(\ln F - \ln|F|\right)/z_0 \tag{3.25}$$

where F is the field value obtained by BPM

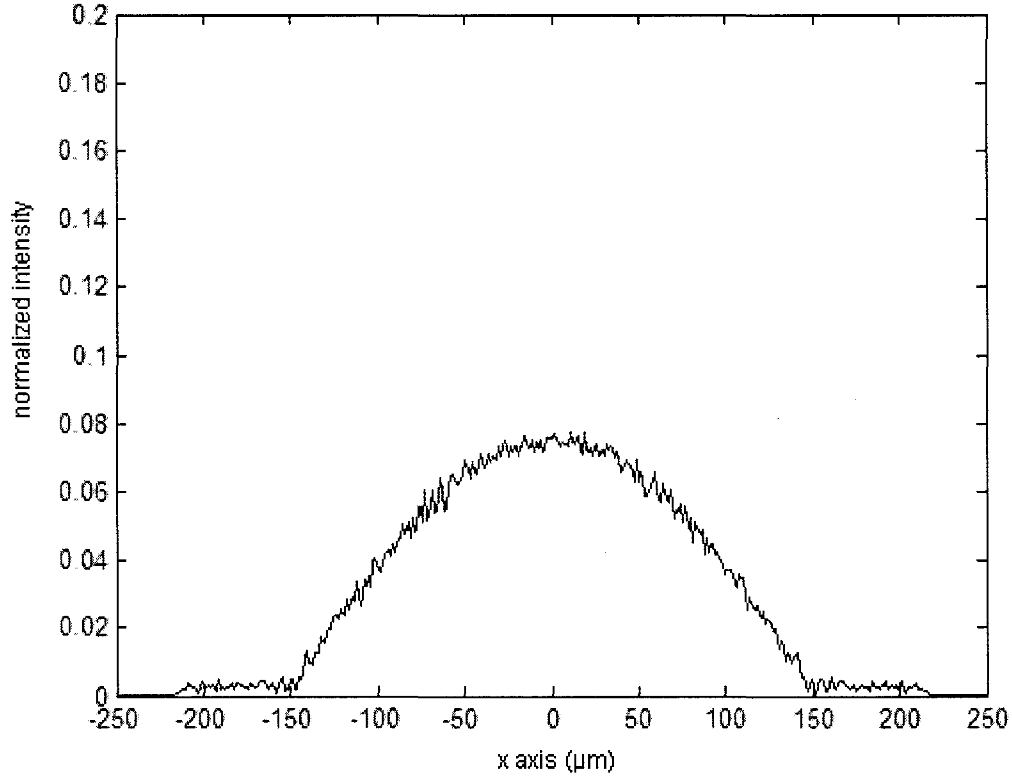

Fig. 3.2 Field intensity after original 1st lens

From Fig. 3.2 & 3.3 we can clearly see that that the output wave is collimated but not like a gate function as desired. In order to achieve that goal, physically, we need to make rays near the propagation axis experience more delays, i.e. increase the value of a. Also we need to take the phase factor into consideration. A phase compensation part is placed right after the lens to make the output wave phase flat.

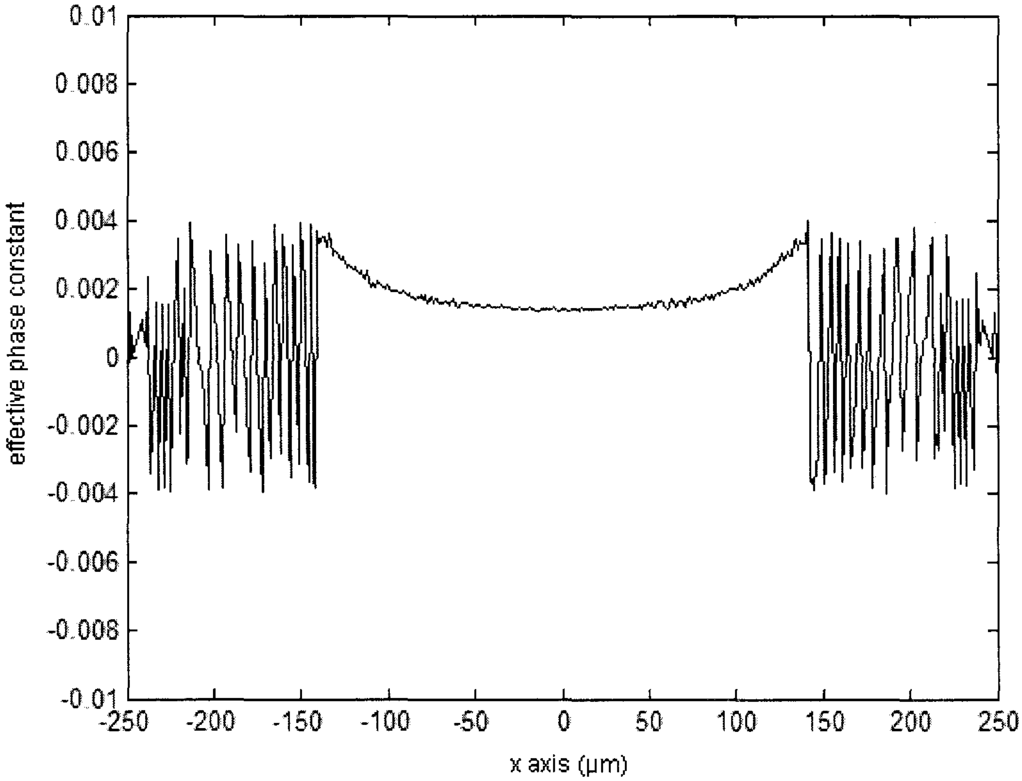

Fig. 3.3 Phase factor after original 1st lens

The schematic diagram of the final design is shown in Fig.3.4.

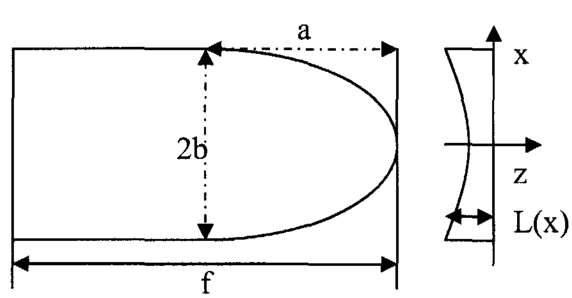

Fig. 3.4 Schematic diagram of 1st lens structure

The design parameters are summarized in Table 3.2.

Parameters	Value (μm)
a	363.85
b	150.35
f	652.8
L(x)	$2.5+1.2\times10^{-4}x^2+4.8\times10^{-9}x^4-1.8\times10^{-13}x^6$

Table 3.2 Parameters for the 1st lens

And the simulation result can be found in Fig. 3.5 & 3.6.

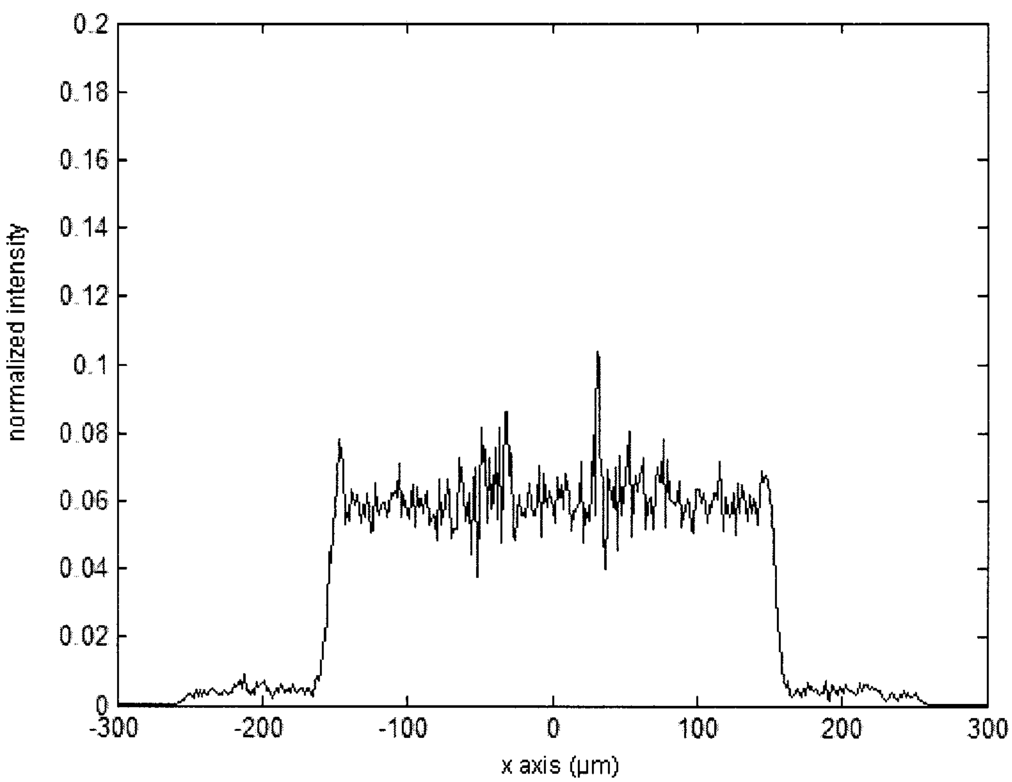

Fig. 3.5 Field intensity after 1st lens

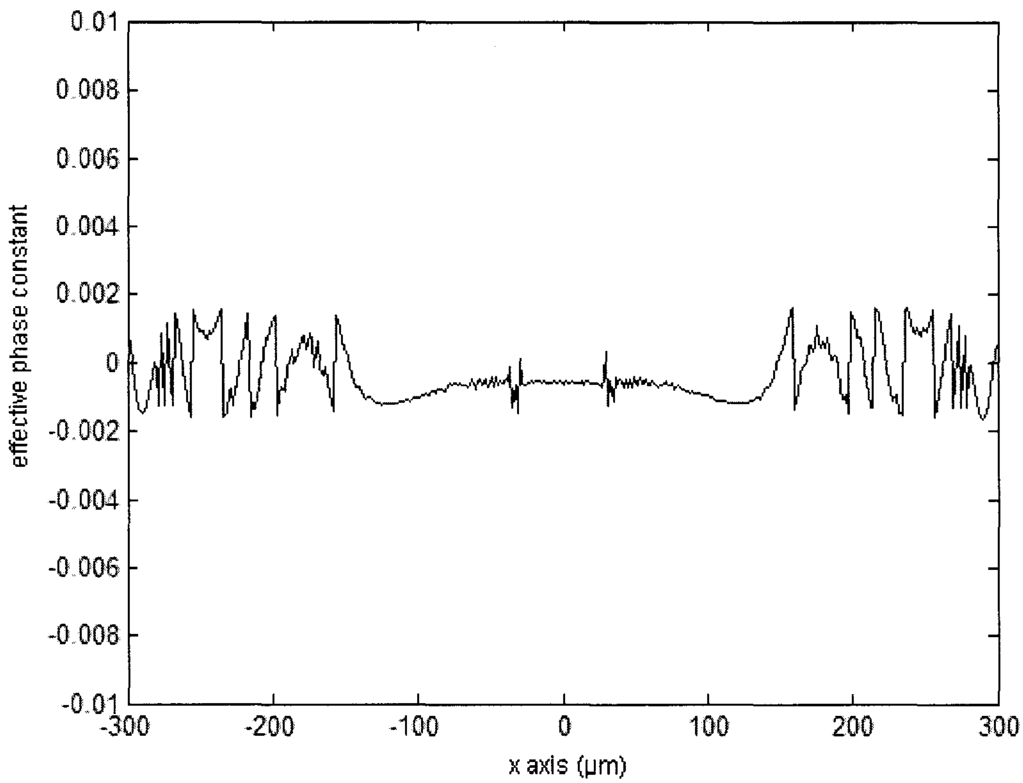

Fig. 3.6 Phase factor after 1st lens

We can see that there are lots of ripples in both amplitude and phase parts. It is inevitable since we are trying to get a gate function like output. It will lead to uniformity problem in our final result. All we can do is to try different sets of parameters and find a compromise between the two. This is the best result we can get so far.

3.3.3 Other Lenses Design

From equation 2.6, we can clearly see that the lens introduces a phase shift to the wavefront and the Fourier transfer is done after a distance of propagation. One of the approximations is that the lens is thin, i.e. only paraxial rays are considered. The length of the lens can be substantially reduced when our attention is restricted to the portion of the wavefront that lies near the lens axis.

The design principle of the lens is shown in Fig. 3.7, where we divide the lens into many pieces and reduce the length of each piece by hundreds of wavelengths. The reason why we do this is that the phase difference introduced by the lens remains the same while we make it much thinner. Specific parameters can be found in table 3.3.

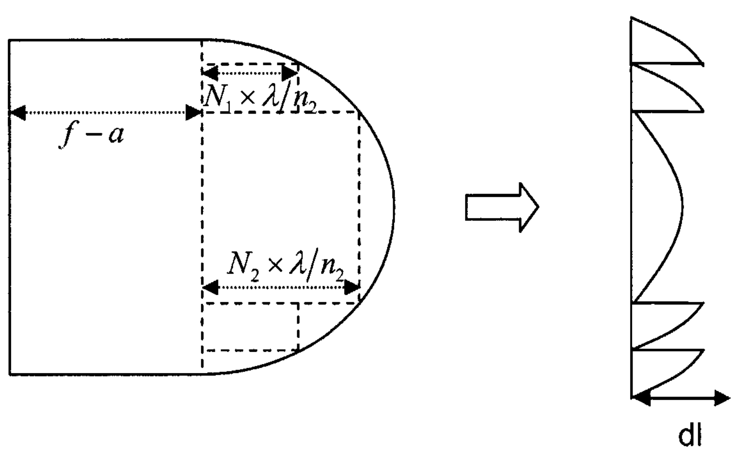

Fig. 3.7 Principle for lens optimize

The lens is based on the structure we proposed in chapter 3.2.1. Now let's consider the structure with two waveguide lenses that both collimating and refocusing the light beam coming from an input waveguide. If the lenses are designed ideally, this light beam which passes through the first lens and then refocuses after the second lens should be totally coupled into the output waveguide. In other words, the minimum insertion loss of such an optical system serves as an important measurement of the lens design. Fig.3.8 shows the field distribution for the two-lens structure. Fig. 3.9 shows the insertion loss for the structure, which is 0.01dB

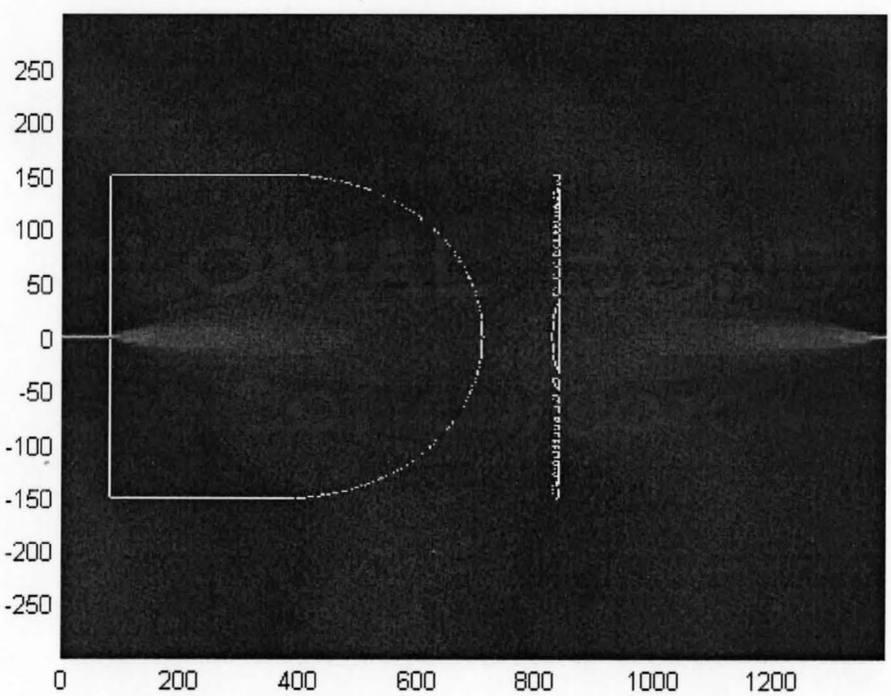

Fig. 3.8 Example of the double lens structure

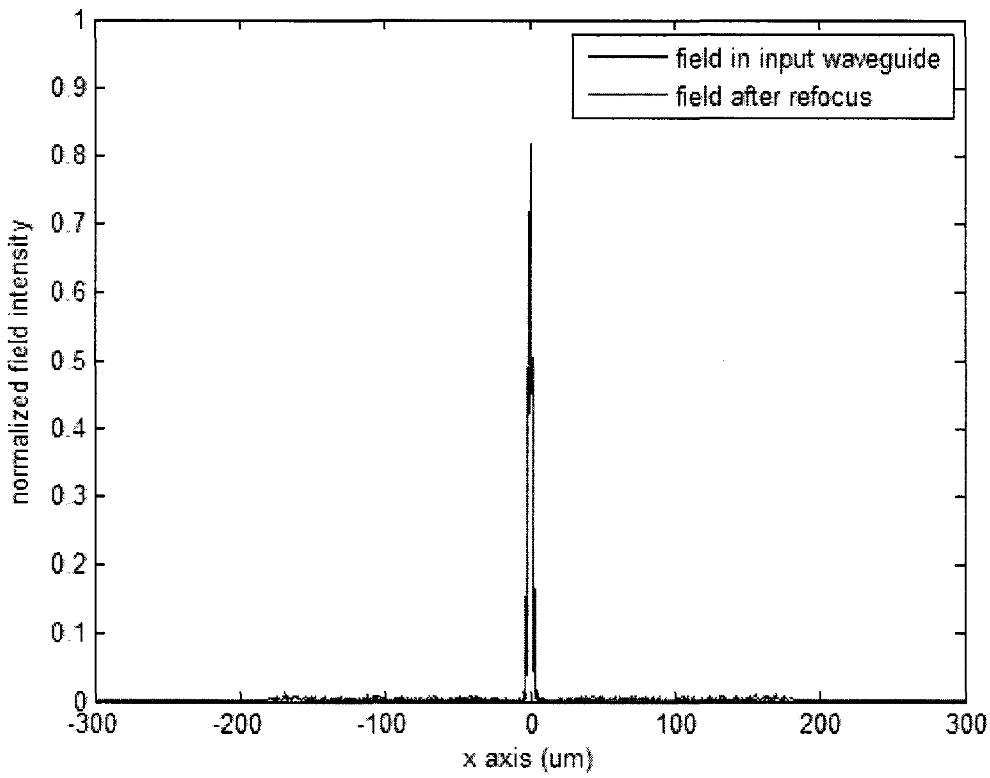

Fig. 3.9 Input field Vs refocused output field

Area 4, 5 and 7 are all using the same structure. Both D and f are 600μm. Lens is divided into 39 pieces and the length is around 28μm. The detailed parameters are shown in table. 3.3

Parameters	Value (μm)
f	600
D	600
N	39
dl	~28

Table 3.3 Parameters for lenses

3.4 1st Phase Grating Design

As previously mentioned, the phase grating (PG) is a key component in this power splitter configuration. The schematic view of the original grating structure is shown in Fig. 3.10

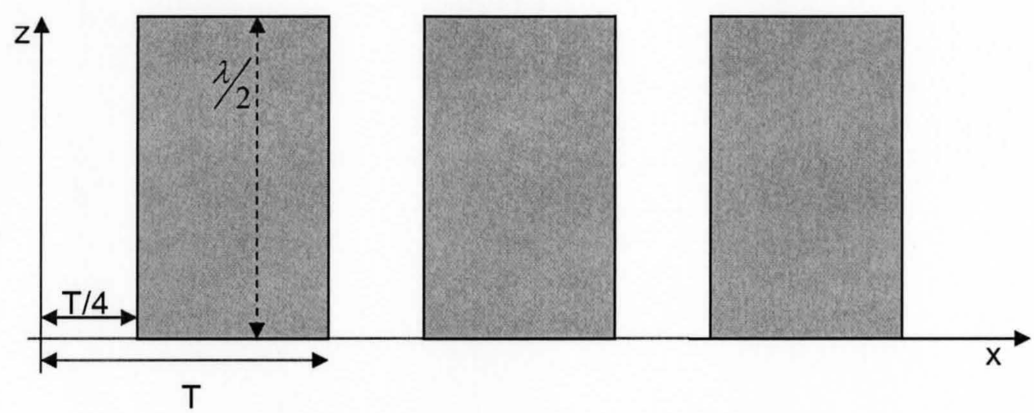

Fig. 3.10 Schematic view of the original grating structure

The PG structure is made of N periods of identical rectangular structure with period T, height $\lambda/2$ and refractive index n_2. The total aperture size is D = NT. For a single period

$$F(x)=\begin{cases} 0, 0 \le x < \dfrac{T}{4} \\ \dfrac{\lambda}{2}, \dfrac{3T}{4} \le x \le T \end{cases} \tag{3.26}$$

It has been proved in the previous section that the incident optical waveguide mode will be collimated and becomes a quasi-plane wave after propagating through the lens. This collimated light beam then experiences a pure phase delay after passing through the PG. For each period, the unit transfer function is, therefore, given by

$$P(x) = Ga\left(\frac{x}{T}\right)\exp\left(j\varphi(x)\right) \tag{3.27}$$

where $\varphi(x) = \begin{cases} 0, 0 \le x < \dfrac{T}{4} \\ \pi, \dfrac{3T}{4} \le x \le T \end{cases}$

Due to the periodicity of the structure, the pupil function satisfies P(x + T) = P(x), which means we can rewrite the pupil function by a Fourier series.

$$P(x) = \sum_{m=-\infty}^{m=\infty} A_m \exp(i2\pi \frac{m}{T} x) \tag{3.28}$$

Where the coefficient A_m is given by

$$
\begin{aligned}
A_m &= \frac{1}{T}\int_0^T \hat{P}(x)\exp(-i2\pi\frac{m}{T}x)dx \\
&= \frac{1}{2}\exp(-i\frac{\pi m}{4})\sin c(\frac{m}{4})
\end{aligned}
\tag{3.29}
$$

With the limited aperture D=NT, where N is the number of period, the pupil function is

$$
P(x) = \sum_{m=-\infty}^{m=\infty} A_m \exp(i2\pi\frac{m}{T}x)Ga(x/D)
\tag{3.30}
$$

After passing through the PG, the collimated light becomes many sub-beams. These beams will be collected by a second lens. As described in the previous section, the inserted lens acts as a spatial Fourier transformer to transform the field at the aperture of the blazed grating to different orders at the focus line. Hence, the field at the focus line can be calculated.

$$
\begin{aligned}
A(v_x) &= FT(P(x)) \\
&= \int_{-\infty}^{\infty} P(x)\exp(-i2\pi v_x x)dx \\
&= D\sum_{m=-\infty}^{\infty} A_m \sin c[D(\frac{m}{T}-v_x)]
\end{aligned}
\tag{3.31}
$$

From the relation between k vector and its x and z components shown in Fig.3.11 it is easy to know that

$$v_x = \frac{n_2 \sin\varphi}{\lambda} \approx \frac{n_2 \tan\varphi}{\lambda} = \frac{n_2 X}{\lambda f} \tag{3.32}$$

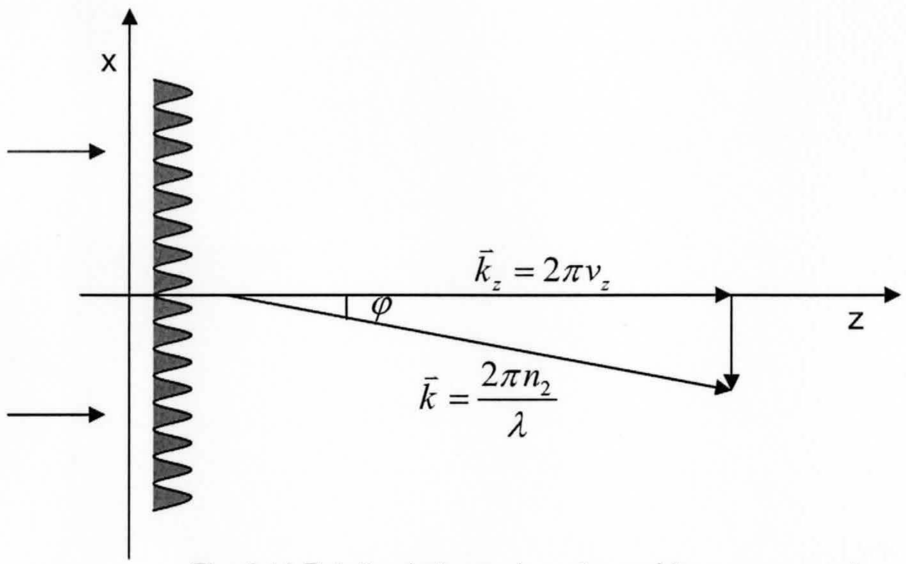

Fig. 3.11 Relation between k vector and its z components

Finally, the approximate imaging field at the focus line is given by

$$A(X) = D \sum_{m=-\infty}^{\infty} A_m \sin c[D(\frac{m}{T} - \frac{n_2 X}{\lambda f})] \tag{3.33}$$

From the equation above we are able to obtain the approximate refocusing position X_m for the m_{th} order blazing light

$$X_m \approx \frac{m\lambda f}{n_2 T} \tag{3.34}$$

Also it is obvious that the amplitude of each order is related to the value of A_m. We calculated the coefficients A_m in different structures (including the original structure described above, triangular one, parabolic one and sinusoidal one). The result is shown in Fig. 3.12. Obviously light would be confined more to the lower orders in the sinusoidal case, which means less loss and smaller lens aperture to capture the light. Fig. 3.12 tells us that the best solution for the phase grating would be the sinusoidal structure.

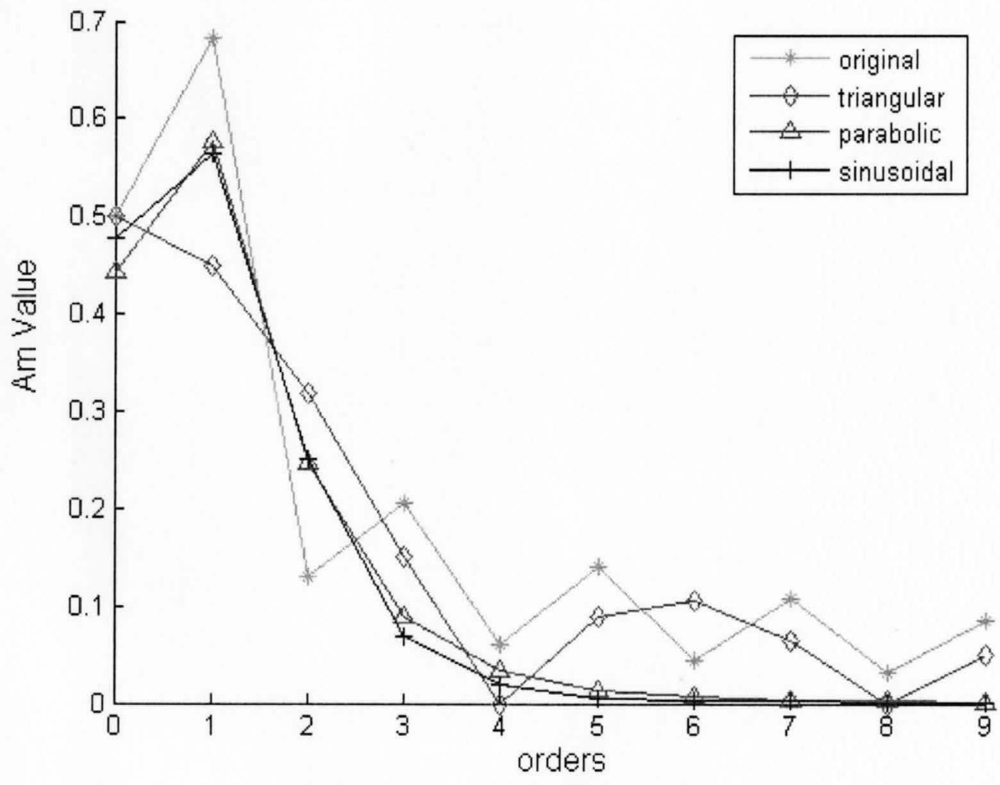

Fig. 3.12 Am for different shapes

A schematic view of the grating structure is shown in Fig. 3.13. Actually there are 2 different half sine waves in each period, one is with the period d, height h, while the other one with period (T-d) and height $\lambda/2$ -h. These 2 parameters control the ultimate output wave shape and the design of the second phase shift.

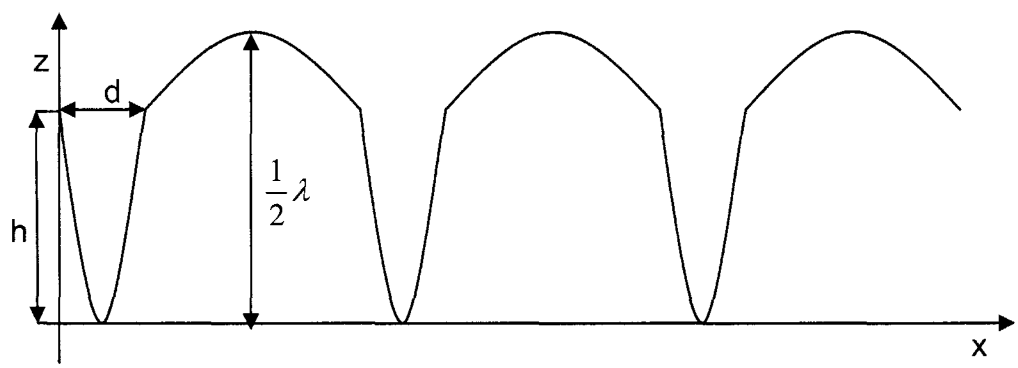

Fig. 3.13 Schematic view of the grating structure

For one single period

$$\hat{F}(x) = \begin{cases} h(1-\sin(\frac{\pi}{d}x)), 0 < x < d \\ (\frac{1}{2}\lambda - h)\sin(\frac{\pi}{T-d}(x-d)) + h, d < x < T \end{cases} \tag{3.35}$$

Then the unit transfer function would be

$$\hat{P}(x)=\begin{cases}\exp[j(\varphi\sin(\frac{\pi}{d}x)-\varphi)],0<x<d\\ \exp\{j[-(\pi-\varphi)\sin(\frac{\pi}{T-d}(x-d))-\varphi]\},d<x<T\end{cases} \tag{3.36}$$

where

$$\varphi=\frac{2\pi h}{\lambda} \tag{3.37}$$

There are two variables, h and d, here. These two parameters are related to each other. Once one of them is fixed, the other can be calculated. We will discuss the value of h first, since it plays an important role in the shape of the output pulse. The coupling efficiency between the output pulse and the mode in output waveguide is a critical judgement here. The output waveguide is chosen as $\Delta n=0.02, width=2.1\mu m$, and d equals to 2 μm. We calculate the output pulse when φ equals to $\frac{5}{8}\pi$, $\frac{6}{8}\pi$, $\frac{7}{8}\pi$, and π respectively, and the mode in the output waveguide as well. The result is shown in Fig. 3.14

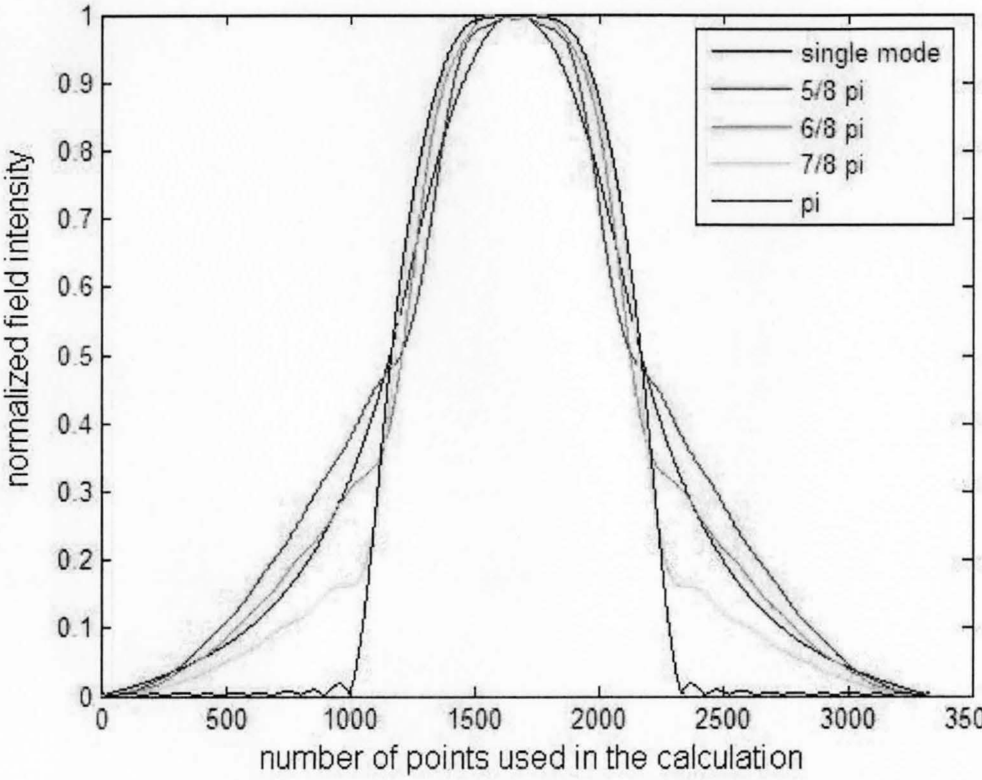

Fig. 3.14 Compare of outcomes and mode in output waveguide

Coupling efficiency is calculated by $efficiency = \left| \frac{\int \varphi_{input} \varphi^{*}_{\sin gle \bmod e} dx}{\int \left| \varphi_{\sin gle \bmod e} \right|^2 dx} \right|$, the result is shown in table 3.4

φ	$\frac{5}{8}\pi$	$\frac{6}{8}\pi$	$\frac{7}{8}\pi$	π
Coupling efficiency	0.926	0.934	0.940	0.938

Table 3.4 Coupling efficiency for different value of φ

The results would be of little difference if we make a little change to the width d (which must be sure to be less than 2.16um). According to equation 3.37,

$$h = \frac{7}{16}\lambda$$

All the parameters are summarized in Table. 3.5. Way to calculate d will be discussed in chapter 3.5

Parameters	Value (μm)
T	8
d	2.785
h	$\frac{7}{16}\lambda$ =0.339

Table 3.5 Parameters for blazed phase gratings

3.5 2nd Phase Shift Design

The design of the 2nd phase shift is relatively simple. It is a rectangular structure with width w along x direction and length l along z direction (Fig. 3.15). The width should be big enough to capture the 0th order light but not too big so the 1st order light would not experience the phase delay. The length determines the amount of delay that should be introduced to the 0th order, and the phase delay can get the light cancelled in the point (say point A) which experienced phase shift π in the PG.

Assume that the average value of the 0th order light to be ae^{ib}. Then the field in point A can be expressed as $-1-ae^{ib}+ae^{ib}$. After the 2nd phase plate, we introduce a phase shift, say θ , to the 0th order part, which means the output in point A would be

$$-1-ae^{ib}+ae^{ib}e^{i\theta}$$

Now we have to make $-1-ae^{ib}+ae^{ib}e^{i\theta}=0$, which gives us

$$e^{i\theta}=\frac{1}{a}e^{-ib}+1 \qquad (3.38)$$

By adjusting d, the parameter ranges from 0 to T, we can find a designable value which makes $\left|\frac{1}{a}e^{-ib}+1\right|=1$. Once we get d, we can easily get the phase shift θ of the 2nd phase plate.

In our case $d=2.69\mu m,\theta=1.63$

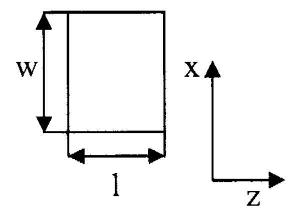

Fig. 3.15 Schematic view of the grating structure

Parameters	Value (μm)
w	38
l	1.542

Table 3.6 Parameters for 2nd phase shift

3.6 Summary

In this chapter, each part of the power splitter is carefully studied and optimized with the help of analytical formulation and numerical simulation. The shape of the 1st lens and the 1st phase grating are the two most important parts of the design. The lenses we designed consist two types, one for gate-function wavefront shaping while the other for phase correcting. We also proposed a sinusoidal period phase grating, which can reduce the insertion loss, and increase the coupling efficiency as well. The performance of the whole device will be presented in the next chapter.

Chapter 4

Numerical Simulation of the Novel Power Splitter

4.1 Introduction

We present the analytical simulation to our device at first, evaluating the performance in ideal situation. Then BPM is employed to simulate the whole device. The size of the power splitter is 600μm (width) by 2700μm (length). The mesh grid we use is 30000 by 90000, which means 50 points per micron in x direction while 33 points per micron in z direction. Insertion loss, uniformity, size and cost are all important parameters to power splitters. Simulation results of loss, uniformity and wavelength dependence will be discussed latter in chapter 4.3 respectively.

4.2 Analytical Simulation

Here we assume that the field after 1st lens is a gate function, which means

$$u_1(x) = Ga(x/D) \tag{4.1}$$

The phase grating uses the exact the same parameters in table 4.5, except that the number of periods is increased to 128. The pupil function can be written as

$$P(x) = \sum_{m=-\infty}^{m=\infty} A_m \exp(i2\pi \frac{m}{T} x) Ga(x/D) \tag{4.2}$$

where A_m can be calculated analytically.

If we assume that our lens is infinite, which means it can perform an exact Fourier transform. After the 2nd lens, the field can be written as

$$\begin{aligned} A(x) &= FT(P(x)) \\ &= \int_{-\infty}^{\infty} P(x) \exp(-i2\pi v_x x) dx \\ &= D \sum_{m=-\infty}^{\infty} A_m \sin c[D(\frac{m}{T} - \frac{x n_h}{f\lambda})] \end{aligned} \tag{4.3}$$

By putting all the parameters into the equation above, we can get the analytical solution of $A(x)$, which is shown in Fig. 4.1.

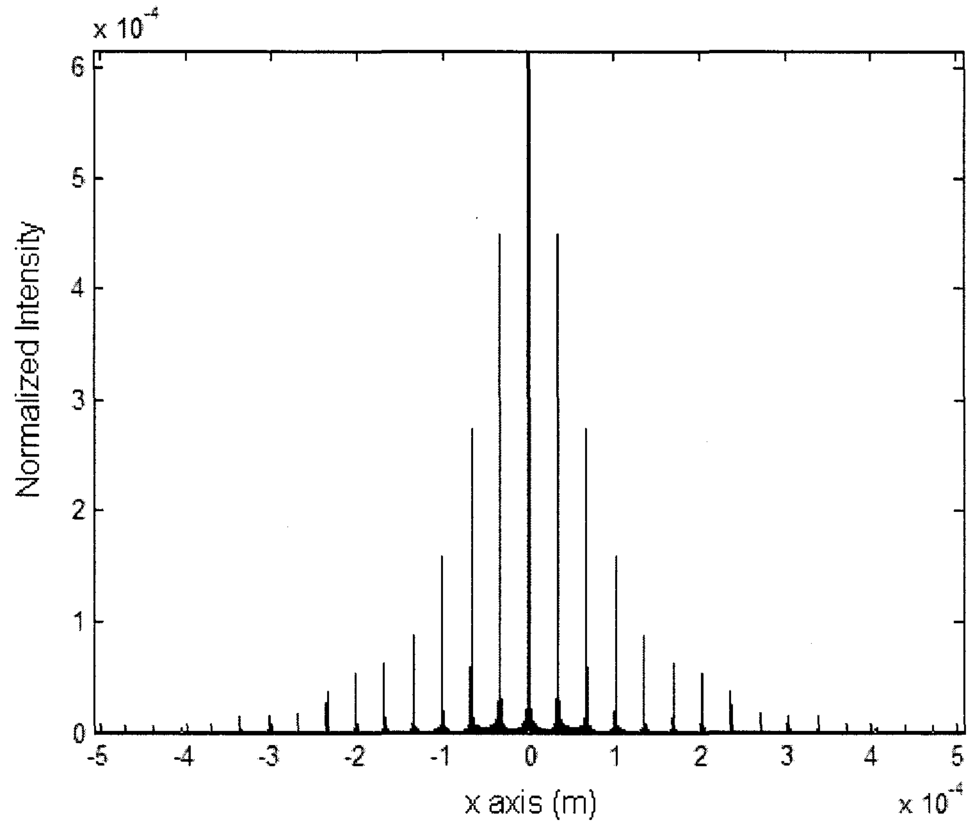

Fig. 4.1 Different orders along the back focal plane of the 2nd lens

Since our 2nd phase only has effect on the DC part, we can simply make A_0 be $A_0 = A_0 \exp(i\theta)$, while the other parts remain unchanged. The 4th lens does another Fourier transformation to the field $A(x)$. And the outcome would be

$$\begin{aligned} B(x) &= FT(A(x)) \\ &= \sum_{m=-\infty}^{m=\infty} A_m \exp(i2\pi \frac{m}{T} x) Ga(x/D) \end{aligned} \tag{4.4}$$

We can also get the figure for $B(x)$ in the same way as we get $A(x)$, the result is shown in Fig. 4.2.

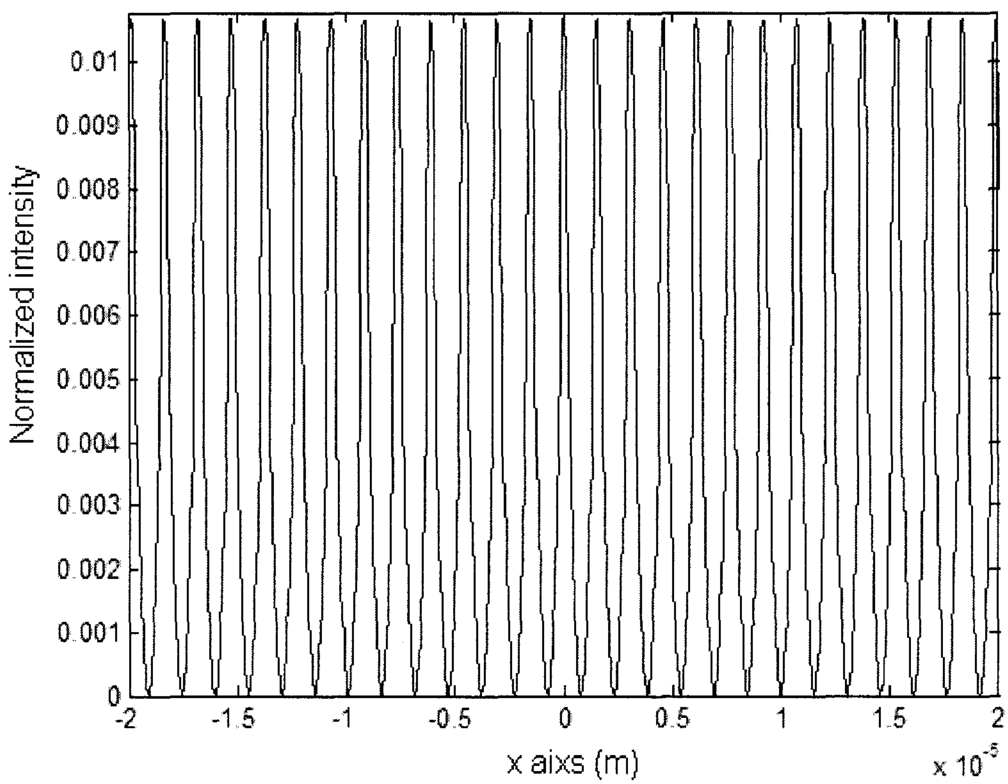

Fig. 4.2 The analytical output field

Evidently, the output field profile is exactly what we want, optical power gets split equally. However, it is the ideal case. One of the approximations we made above is that the lens is assumed to be infinite, while in reality it is impossible. If we make the aperture of the lens be 600 μm, which means we can only confine orders less than the 9^{th}, and accordingly, we make the number of channels be 32, the insertion loss comes out. More important thing is that the Fourier transform of the limited orders would not be the same as in Fig. 4.2. The FT result of the limited field is shown in Fig. 4.3. The loss is calculated to be 0.014dB.

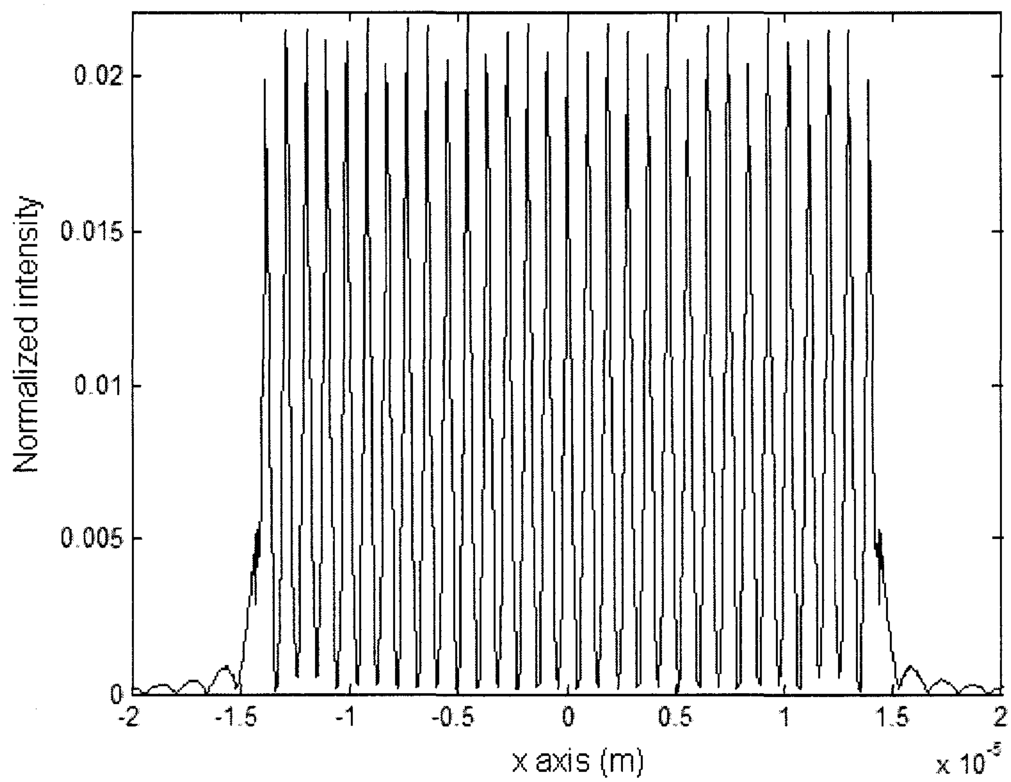

Fig. 4.3 Output field when considering the aperture of the lens

Fig. 4.3 tells us that the uniformity depends on two aspects. One is the output of the first lens, that is, how close can the collimated be like a gate function. The other is the aperture of the lens, that is, how many orders can be captured.

As we discussed before, the sinc function determines the position of each order. If we make the period of the phase grating larger, say, 16 μm, we can find that lens can capture more light compared to 8 μm case, as shown in Fig. 4.4. However, the change on the phase grating means the output waveguide should change accordingly, the coupling efficiency will decrease. The full width at half maximum (FWHM) for 8 μm case is 2.76 μm, while for 16 μm case it becomes 5.94 μm. The width of the period is a compromise between the insertion loss and coupling efficiency.

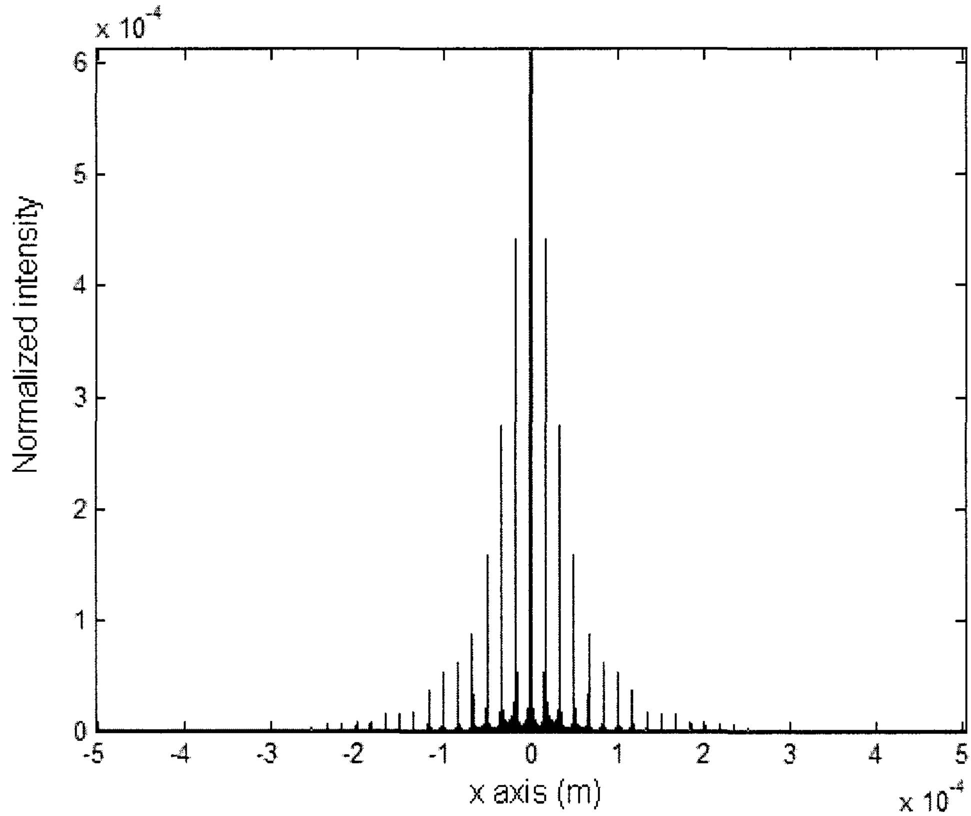

Fig. 4.4 Order distribution when the width of the period is 16 μm

4.3 BPM Simulation Results for 32-Channel Power Splitter

4.3.1 Insertion loss

A schematic structure of this power splitter is shown in Fig.4.5

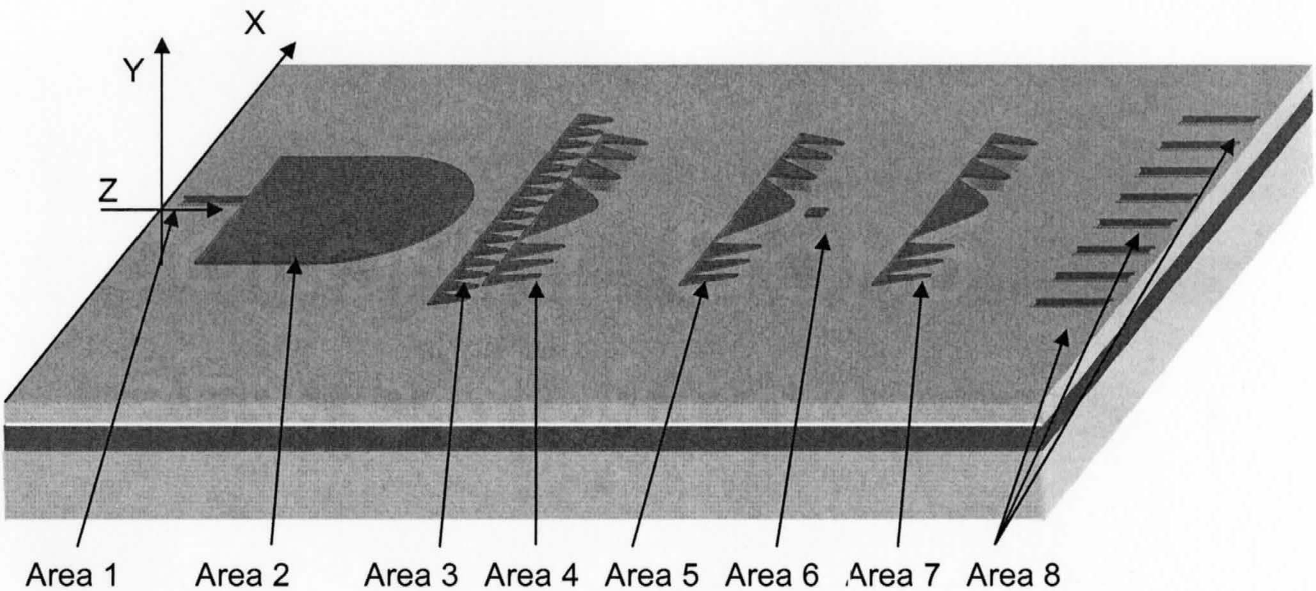

Fig. 4.5 3D view of the whole device

Once the layout is set and the parameters are determined, we used a 2-D beam propagation method to predict the device performance and obtained the top view field distribution, as shown in Fig. 4.6.

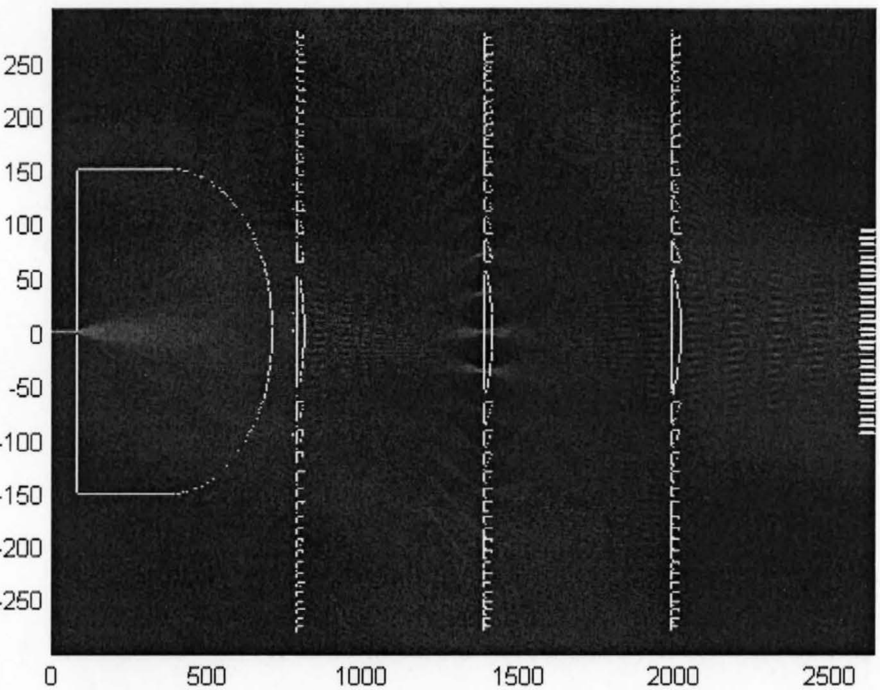

Fig. 4.6 Top view of the field distribution

We can clearly see that the wave gets collimated after the 1st lens, and splits into different orders in the back focal plane of the 2nd lens as we expected. Finally, the wave gets split into many channels along the focal line of the last lens, where the output waveguides are placed.

The field distribution right on the focal plane of the 2nd lens is shown in Fig. 4.7. And the output field is given in Fig. 4.8.

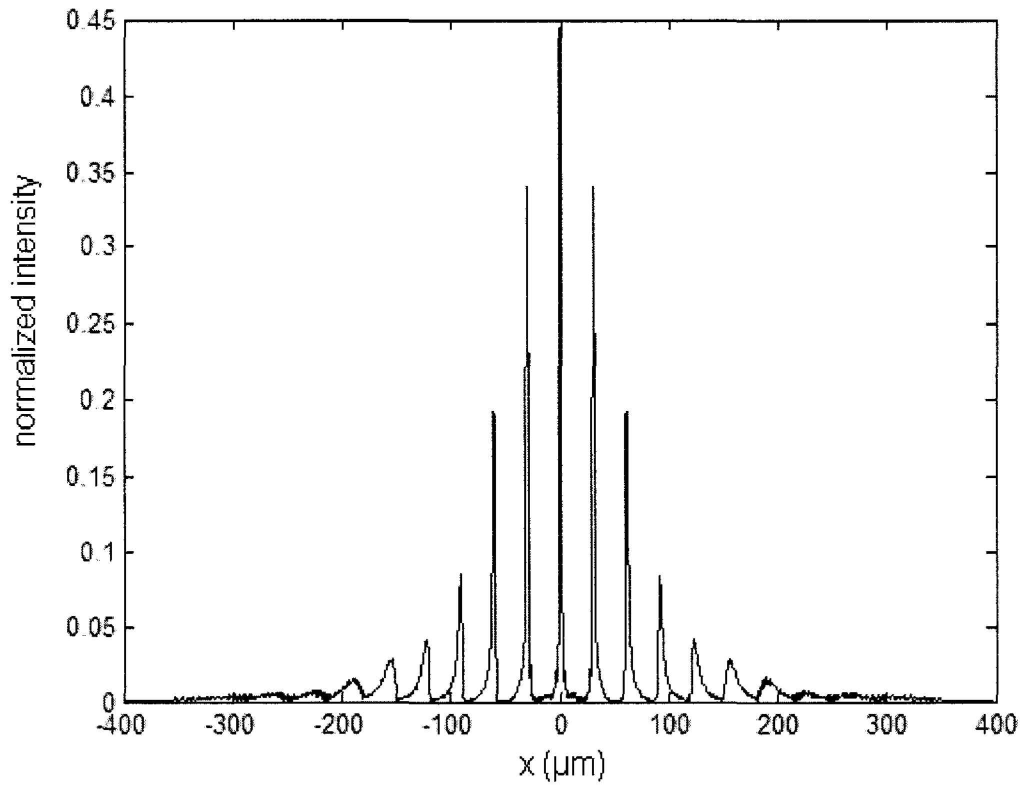

Fig. 4.7 Field distribution at the focal plane of the 2nd lens

The loss is calculated by the ratio between power in 32 channels and input power, $loss = 10\log\left(\frac{P_{out}}{P_{in}}\right)$, which comes out to be 0.219dB, which means around 94.4% of the input power coupled into the output channels.

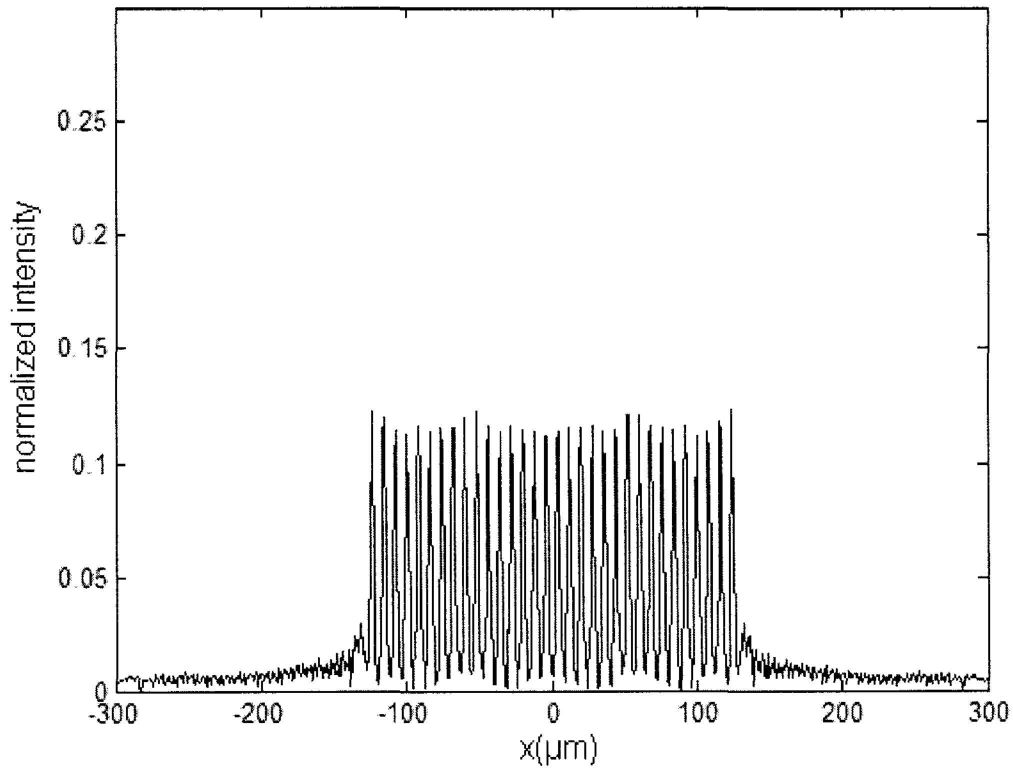

Fig. 4.8 Output field

4.3.2 Uniformity & Coupling efficiency

The map of uniformity is shown in Fig. 4.9. It shows the ratio between the power in each channel and the average power. The maximum ratio is around 1.05. The profile of Fig. 4.9 is mainly determined by the collimated light shown in Fig. 3.5.

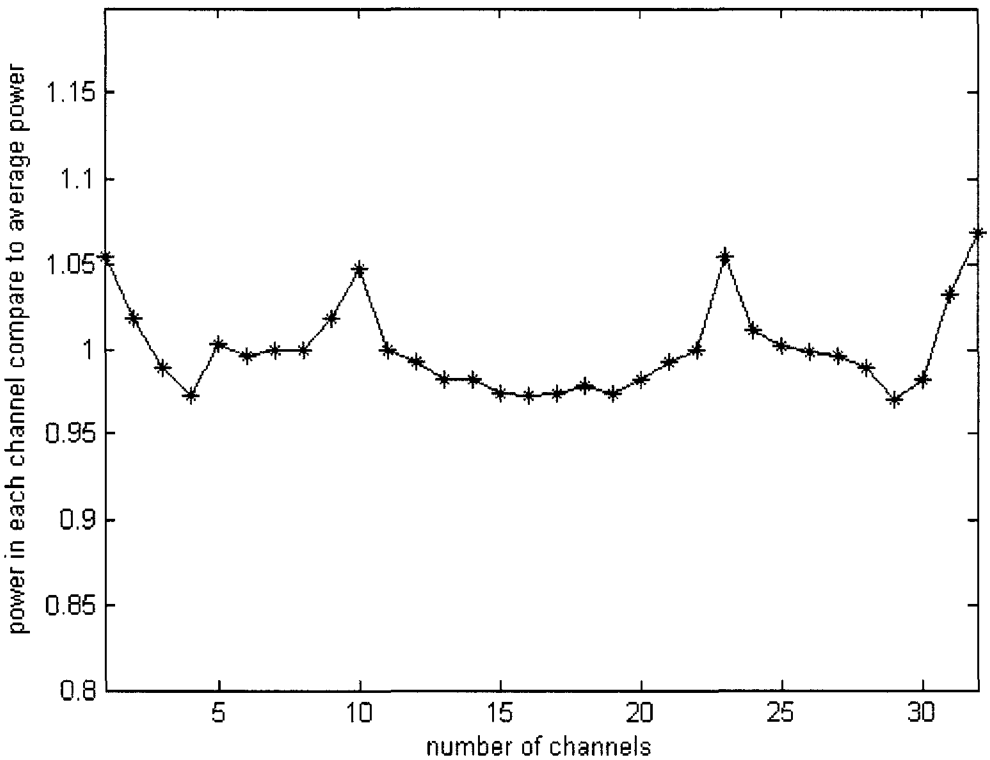

Fig. 4.9 Uniformity result

Coupling efficiency between the field on the back focal plane of the last lens and the output channels is one of the major causes of the insertion loss in this device. Theoretical calculation was discussed on chapter 3.3. The coupling coefficient is expected to be around 94%. Here I select No. 1 8 16 channel of the right half in my calculation here (Fig. 4.10). The blue ones are field distribution amplified from Fig. 4.8, while the red ones are the theoretical mode profile. The coupling efficiency is shown in table 4.1.

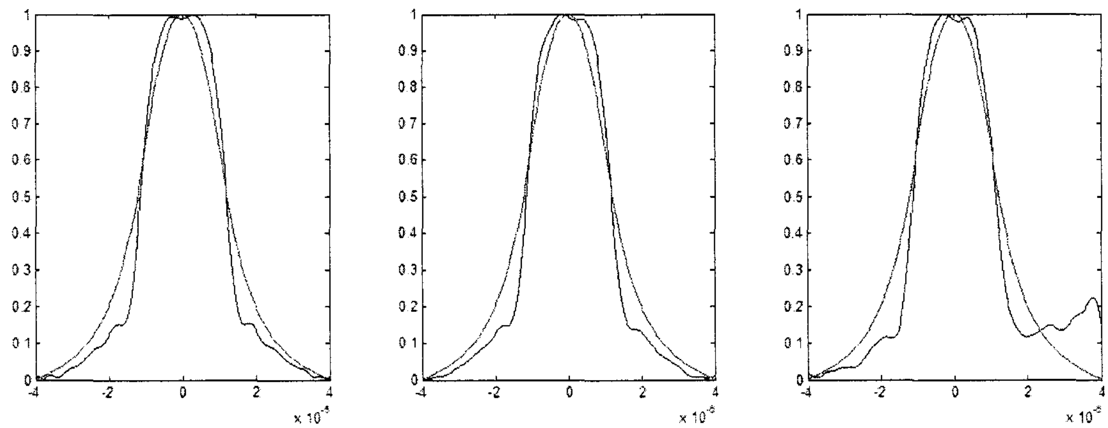

Fig. 4.10 Output in No. 1 8 16 channels

Channel number	1	8	16
Coupling coefficient	92.1%	92.0%	89.2%

Table 4.1 Coupling coefficient for each channel

4.3.3 Wavelength Dependence

Change in wavelength does not have much effect on the insertion loss and coupling coefficient but it would change the power in each channel. Since the design of the 1st lens is specific for 1.55 μm, other wavelengths cannot get collimated.

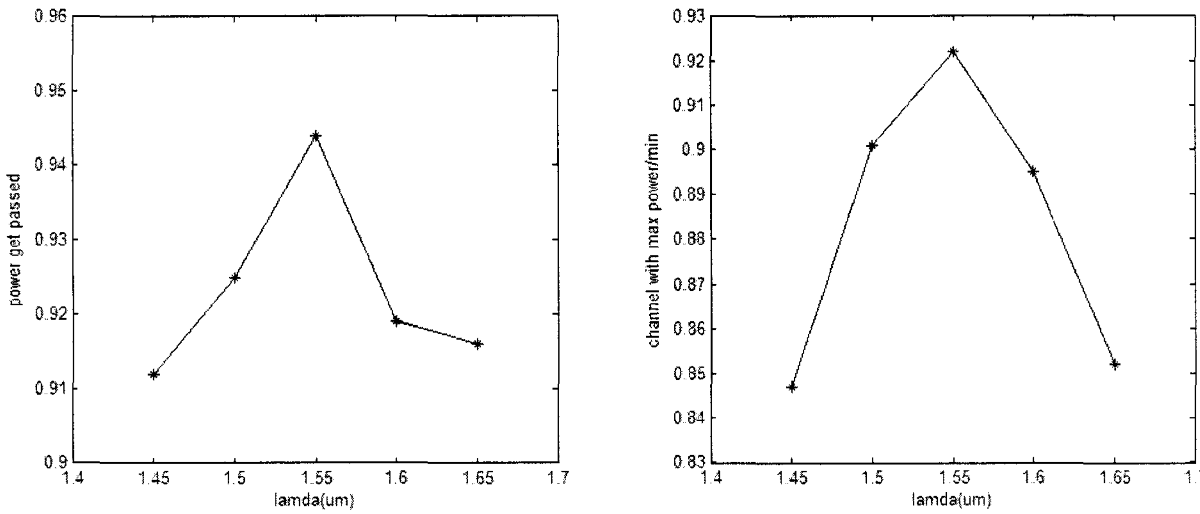

Fig. 4.11 Insertion loss and uniformity issues for different wavelength

4.4 BPM Simulation Results for 64-Channel Power Splitter

We can extend the number of output channels to 64 or 128 or any channels we want, just by expending the width of the device and redesigning of the lenses, while the length of the device remains the same.

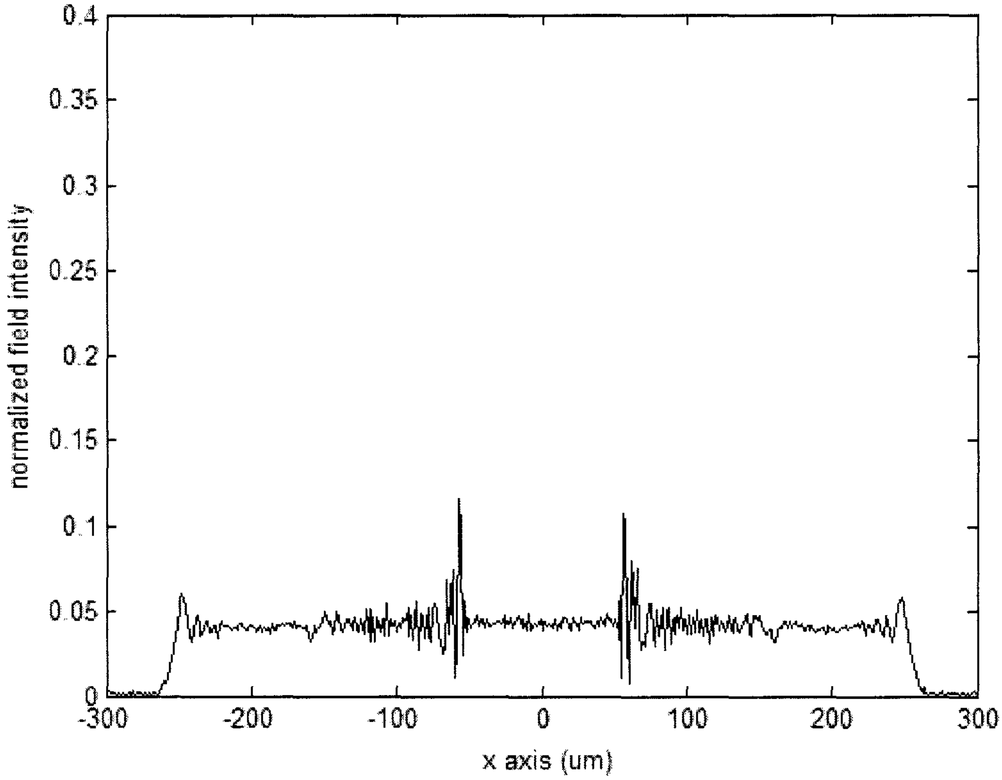

Fig. 4.12 field intensity after 1st lens – 64-channel case

Here are some results for the 64-channel case. The normalized intensity after 1st lens is shown in Fig. 5.12, while the output at the back focal plane of the 4th lens is shown in Fig. 5.13

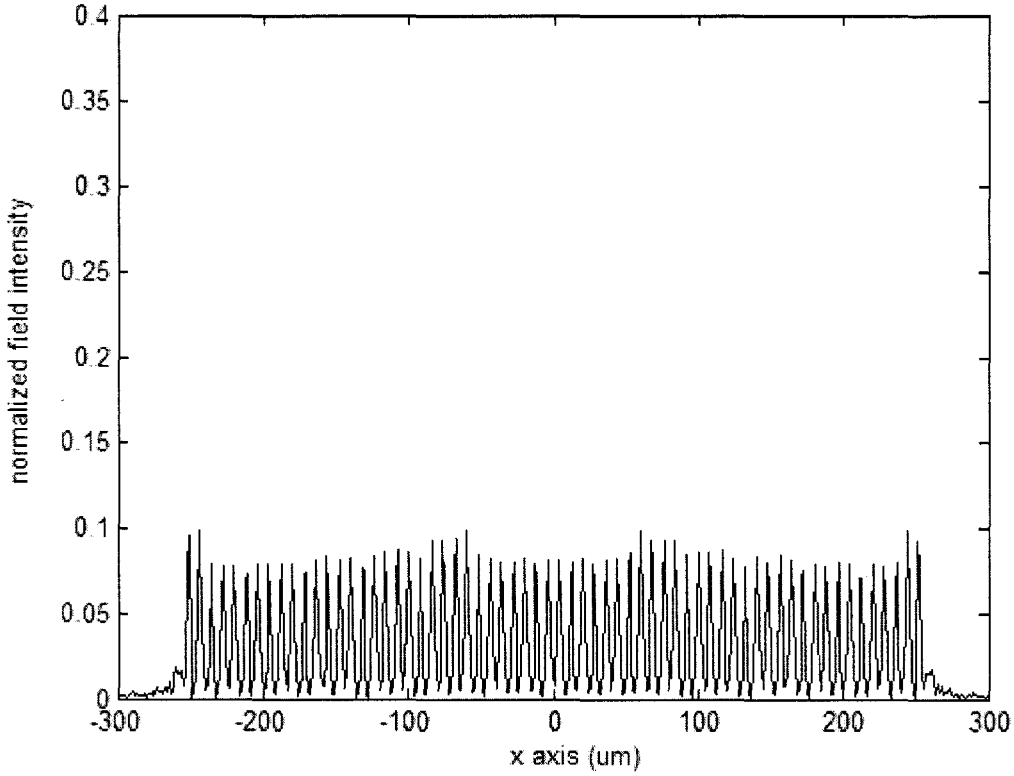

Fig. 4.13 Output field – 64 channel case

The insertion loss for 64-channel case is similar to the 32-channel case, but the uniformity result is worse, which can be seen in Fig. 4.14.

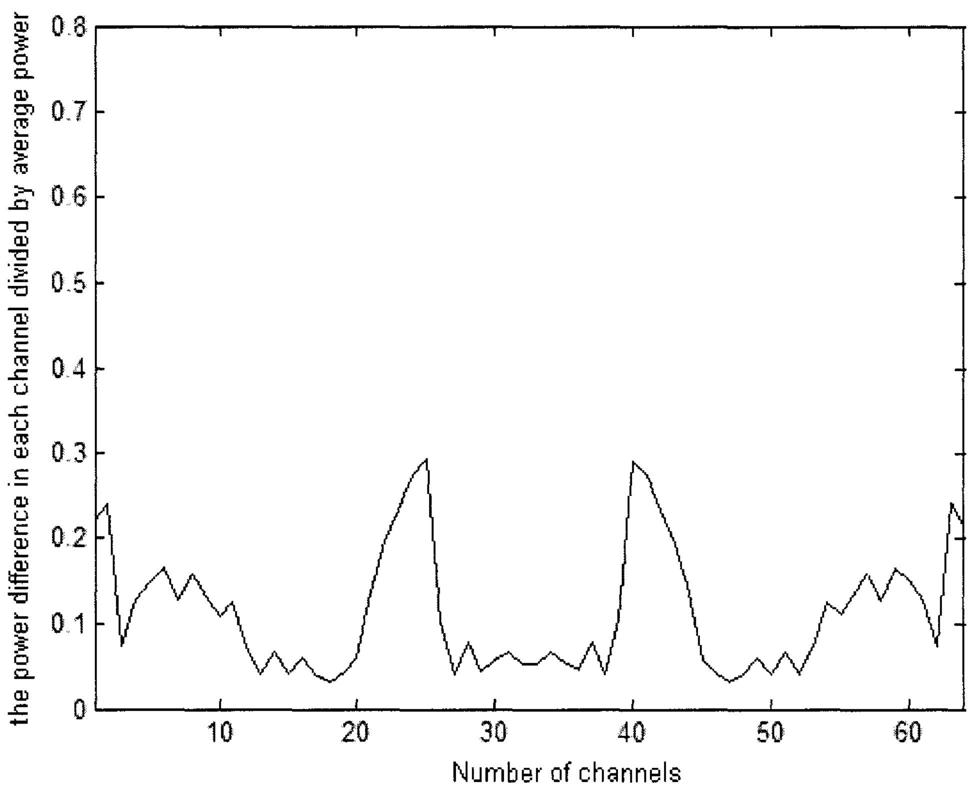

Fig. 4.14 Uniformity result for 64-channel case

4.5 Summary

In this chapter, we have verified the new design for planar integrated power splitter by combing four carefully designed waveguide lenses and two phase gratings. Insertion loss around 0.2dB can be achieved with the novel device. Compare to conventional MMI structure, the design presented here has the potential of reducing device size.

Chapter 5

Conclusion

5.1 Summary

Here we design and simulate a power splitter based on a newly proposed planar waveguide structure. The insertion loss is around 0.2dB. The whole device is about 600μm (width) by 2.7mm (in length). It is also possible to make a 64 channel power splitter of the same size by redesigning the lenses.

Our design can greatly reduce the device size compared with currently deployed power splitters. Also we can potentially reduce the cost.

5.2 Suggestion on Future Research Direction

Neither 3D effects nor the edge reflections were considered in our design and simulation, also the polarization dependence is a potential problem of the design. All these problems will be our future research tasks.

Bibliography

[1] "Access Network Systems: North America— Optical Access. DLC and PON Technology and Market Report," *RHK-RPT-0548, RHK Telecommun. Industry Analysis* San Francisco, CA, June 2001.

[2] J. W. Arkwright, D. B. Mortimore, and R. M. Adnams, "Monolithic 1 x 19 singlemode fused fiber couplers," IEE Electron. Lett., vol. 27, no. 9, pp. 737-738, 1991.

[3] N. Nourshargh, E. M. Starr, and T. M. Ong, "Integrated optic 1 x 4 splitter in SiOz/GeOa," IEE Electron. Lett., vol. 25, no. 15, pp. 981, 982, 1989.

[4] Yasuhiro Hida, Yasuyuki Inoue, Fumiaki Hanawa, Takao Fukumitsu, Yoshitaka Enomoto, and Norio Takato, "Silica-Based 1 32 Splitter Integrated with 32 WDM Couplers Using Multilayered Dielectric Filters for Fiber Line Testing at 1.65 μm" IEEE PHOTONICS TECHNOLOGY LETTERS, VOL. 11, NO. 1, JANUARY 1999

[5] S. Day, R. Bellerby, G. Cannell, and M. Grant, "Silicon based fiber pigtailed 1 x 16 power splitter," IEE Electron. Letter, vol. 28, no. 10, .pp 920-922, 1992.

[6] L. Soldano, F. B. Veerman, M. K. Smit, B. H. Verbeek, A. H. Dubost, and E. C. M. Pennings, "Planar monomode optical couplers based on multimode interference effects," J. Lightwave Technol., vol. 10, no. 12, pp. 1843-1850, 1992.

[7] M. A. Fardad and M. Fallahi, "Sol-Gel Multimode Interference Power Splitters" IEEE PHOTONICS TECHNOLOGY LETTERS, VOL. 11, NO. 6, JUNE 1999

[8] L.B. Soldano, E.C.M. Pennings, Optical multi-mode interference devices based on self-imaging: principles and applications, J. Lightwave Technol. 13_1995.615–627.

[9] Rui Yin, Jianyi Yang, Xiaoqing Jiang, Jin Li, Minghua Wang, "Improved approach to low-loss and high-uniformity MMI device" Optics Communications 181_2000.317–321

[10] J. W. Goodman, Introduction to Fourier Optics, McGraw-Hill Science, 2nd edition, 1996.

[11] S. Sinzinger and J. Jahns, Microoptics, 2nd ed. (Wiley-VCH, Weinheim, 2003)

[12] B. R. Brown and A.W. Lohmann, Complex spatial filtering with binary masks, Appl. Opt. 5, 967–969 (1966).

[13] T. J. McHugh and W. B. Veldkamp, Binary optics, Sci. Am. 266, 92–97 (1992)

[14] B. Broberg and S. Lindgren, "Refractive index of In1−xGaxAsyP1−y layers and InP in the transparent wavelength region" J. Appl. Phys. 55, 3376 (1984);

[15] K. Okamoto, Fundamentals of Optical Waveguides, San Diego, CA: Academic, 2000

[16] M. D. Feit and J. A. Fleck, Jr., "Light propagation in graded-index optical fibers" Applied Optics, vol. 17, no. 24, pp. 3990-3998, 1978

[17] Kenji Kawano, Tsutomu Kitoh, Introduction to Optical Waveguide Analysis: Solving Maxwell' S Equation and the Schrö Dinger Equation, John wiley & sons, INC, 2001

[18] B. M. A. Rahman, F. A. Fernandez, and J. B. Davies, "Review of finite

element methods for microwave and optical waveguides," Proc. IEEE, vol.79, pp.1442-1448, 1991.

[19] J. Van Roey, J. van der Donk, and P. E. Lagasse, "Beam-Propagation Method: Analysis and Assessment," J. Opt. Soc. Am.71, 803-810 (1981).

[20] W. P. Huang, Ed., "Methods for modeling and simulation of guided-wave optoelectronic devices: Part II: Waves and Interactions," Progress in Electromagnetics Research, EWM Publishing, Cambridge, MA, 1995.

[21] N. -N. Feng, G.-R. Zhou and W.-P. Huang, "An efficient split-step time domain beam propagation method for modeling of optical waveguide devices," IEEE J. Lightwave Technol., vol.23, no. 6, pp.2186-2191, Jun. 2005.

[22] N. -N. Feng, Modelling, Simulation and Design Techniques for Highdensity Complex Photonic Integrated Devices and Circuits, Ph.D Thesis, McMaster University, Hamilton, ON, Canada, Apr. 2005.

[23] M. Born, E. Wolf, Principle of Optics, Cambridge University Press, 1999.

[24] Stefan Sinzinger, Jürgen Jahns, Microoptics (2nd Edition), Wiley-VCH, 2003

[25] Xun Li, Gui-Rong Zhou, Ning-Ning Feng, and Weiping Huang, "A Novel PlanarWaveguideWavelength Demultiplexer Design for Integrated Optical Triplexer Transceiver" IEEE PHOTONICS TECHNOLOGY LETTERS, VOL. 17, NO. 6, JUNE 2005